Long-Wavelength, Reaction-Based, Fluorescent Sensors for HNO and Mobile Zinc

by

Alexandra T. Wrobel

Submitted to the Department of Chemistry
in supplement to requirements for the degree of

Bachelor of Science in Chemistry

at the

MASSACHUSETTS INSTITUTE OF TECHNOLOGY

June 2014

Author: Signature redacted
Department of Chemistry
May 9, 2014

Certified by: Signature redacted
Stephen J. Lippard
Arthur Amos Noyes Professor of Chemistry
Thesis Supervisor

Approved by: Signature redacted
Rick L. Danheiser
Arthur C. Cope Professor of Chemistry
Undergraduate Officer, Department of Chemistry

Long-Wavelength, Reaction-Based, Fluorescent Sensors for HNO and Mobile Zinc

by

Alexandra T. Wrobel

Submitted to the Department of Chemistry on May 9, 2014

Abstract

Chapter 1. Introduction
A variety of inorganic molecules and ions participate in complex biological signaling networks. Three of these species are nitric oxide (NO), nitroxyl (HNO), and mobile zinc. Maintaining the homeostasis of these signaling molecules is vital and a deeper comprehension of their roles could help in understanding the pathology of specific diseases associated with their dysregulation. One method used to monitor levels of these analytes in biological samples is fluorescence microscopy. Shifting the fluorescence emission to longer wavelengths would improve these already existing probes. Having access to red and near-infrared (NIR) sensors is particularly useful for investigating the interplay of multiple analytes using fluorescence microscopy in conjunction with other probes that emit at shorter wavelengths.

Chapter 2. Synthesis and Characterization of a Fluorescent Sensor with a Dihydrothioxanthene Fluorophore and a Quinoline Based Cu(II) Binding Site
A NIR probe designed to detect NO was synthesized and its photophysical properties were fully characterized. Analysis of the photophysics of this sensor revealed that the quinoline-binding site might be quenching the fluorescence of the fluorophore and preventing a turn-on response upon addition of NO.

Chapter 3. Synthesis, Characterization, and Implementation of a Near-Infrared Fluorescent Sensor for Detection of Nitroxyl (HNO)
A NIR sensor for the detection of HNO was synthesized, fully characterized, and used in live HeLa cells to detect exogenously applied HNO. This probe is selective for HNO over thiols and many other biologically relevant analytes. This sensor was used in combination with the green, zinc-specific probe ZP1 to investigate the relationship between exogenously applied HNO and the release of mobile zinc in HeLa cells.

Chapter 4. Characterization and Targeting of a Red Zinc Sensor
To investigate the levels of mobile zinc in specific cellular organelles, attempts were made to target a red zinc-specific probe to acidic vesicles, the mitochondria, and the nucleus. A combination of peptide-based and small molecule-based targeting approaches was explored, including the vesicle-targeting R9 peptide, the mitochondria-targeting triphenylphosphonium ion, and the DNA-binding Hoechst dye.

Thesis Supervisor: Professor Stephen J. Lippard
Title: Arthur Amos Noyes Professor of Chemistry

Acknowledgements

I would first like to thank Professor Stephen J. Lippard for giving me the opportunity to join his lab at the beginning of my sophomore year. Working in the Lippard Lab has been a wonderful and rewarding experience for me. I have learned so much over the past three years and I am incredibly grateful for the guidance and encouragement I have received within his lab.

I would also like to thank Pablo Rivera-Fuentes, my UROP mentor who supervised all of the work presented in this thesis. He has taught me so much about chemistry and research and has helped me in many other ways. I am very appreciative of the significant amount of time and energy that he devoted to teaching and working with me. The guidance that I received from Pablo has really made my undergraduate research experience enjoyable and fulfilling.

My former UROP mentor within the Lippard Lab, Alexandria (Ali) Liang, has also been a fantastic teacher, role model, and friend. Working with Ali fueled my initial excitement about chemistry and research. I don't think I could ever thank her enough for her constant support and willingness to help me whenever I needed it.

Many other members of the Lippard Lab have also been incredibly helpful, insightful, and a pleasure to work with, including Timothy Johnstone, Robert Radford, Jacob Goldberg, Kogularamanan (Rama) Suntharalingam, and Eric Victor.

And finally, I would like to thank my parents and my two brothers for their support, both personally and academically.

Table of Contents

List of Figures

Chapter 1

Chapter 2

Chapter 3

Chapter 4

List of Schemes

Chapter 1

Chapter 2

Chapter 3

Chapter 4

List of Tables

Chapter 2

Chapter 3

Chapter 1 Introduction

1.1 Biological Relevance of Nitric Oxide, Nitroxyl, and Mobile Zinc

Many inorganic ions and molecules are essential in biological systems.[1] These molecules and metals serve a variety of functions, one of which is the participation in complex signaling networks that regulate and control cellular processes. Three inorganic species of interest are nitric oxide (NO), nitroxyl (HNO), and zinc (Zn^{2+}). In the immune system, NO is released by macrophages during immune response.[2] NO also regulates smooth muscle relaxation within the cardiovascular system and may serve as a neurotransmitter.[3,4,5] HNO, the one electron reduced and protonated form of NO, may be biologically relevant in the cardiovascular and nervous systems, but endogenous production of HNO remains to be conclusively demonstrated.[6] Exogenously applied HNO increases heart muscle contractility and inhibits platelet aggregation.[7,8,9] HNO also appears to be harmful by increasing ischemia-related injury and inducing neurotoxicity.[10,11]

NO and HNO are characterized by distinct biological activity and chemical reactivity.[12,13] In biological systems, HNO acts as both an electrophile and a nucleophile. As an electrophile, HNO can oxidize thiols and, as a nucleophile, HNO can coordinate and reduce metal ions.[14] NO, a free radical, reacts rapidly with other species that contain unpaired electrons, such as heme iron and superoxide.[15,16,17]

In mammals, NO is synthesized via nitric oxide synthase (NOS), a heme-containing enzyme present in three distinct isoforms located in the nervous, cardiovascular, and immune systems. NOS catalyzes the oxidation of L-arginine to citrulline and NO.[15,16,17] Several biosynthetic pathways have been proposed for the generation of HNO and are summarized in Scheme 1.1. One of these proposed pathways

Scheme 1.1. Proposed biosynthetic pathways to HNO

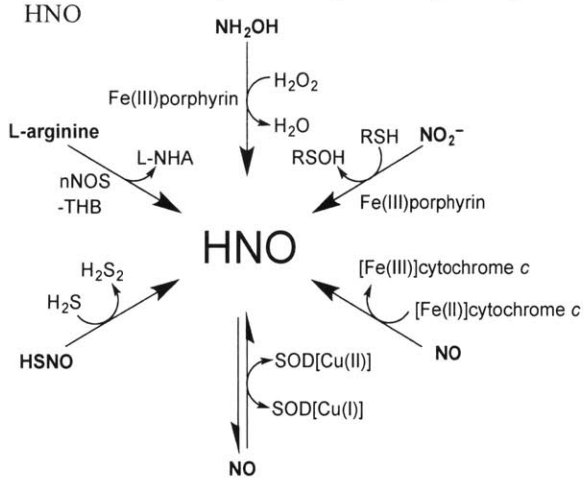

is via NOS. Isolated neuronal NOS (nNOS), one of the isoforms of NOS, produces HNO instead of NO in the absence of the tetrahydrobiopterin (THB) cofactor.[18,19] HNO is also generated through the oxidation of hydroxylamine (NH_2OH) by heme-containing proteins.[20] Superoxide dismutase (SOD) can interconvert NO and HNO reversibly[21] and cytochrome *c* is able to reduce NO to HNO.[22] Reaction between H_2S and HSNO also produces HNO,[23] as well as the reduction of nitrite with H_2S by heme-iron complexes.[24]

Similarly, zinc, a divalent and redox inactive metal in biology, displays distinct and multifaceted roles.[25] Most biological zinc is tightly bound to a variety of metalloproteins. This bound form stabilizes protein structure and participates in catalysis.[26] In addition to zinc incorporation into metalloproteins, zinc occurs in intracellular pools of readily chelatable ions. This loosely bound, or mobile, form of zinc is particularly significant in the brain, prostate, and pancreas. Within the nervous system, mobile zinc is located in presynaptic glutamatergic vesicles and its release is associated with synaptic plasticity.[27] In pancreatic beta cells, zinc is essential for insulin metabolism, crystallization, and release.[28] Additionally, decreased levels of mobile zinc have been associated with the development of prostate cancer.[29]

Maintaining the homeostasis of inorganic molecules and metal ions is vital and its dysregulation is often associated with numerous diseases. For example, up- or down-

regulation of NO production is linked to diabetes, stroke, Alzheimer's disease, and cancer.[30,31,32] Similarly, decreased levels of mobile zinc are also associated with Alzheimer's disease, diabetes, and prostate cancer.[27] The precise role of HNO in disease, if any, remains incompletely understood.[6]

To understand the biological signaling functions of NO, HNO, and mobile zinc, it is important to develop methods and tools to detect these species in live cells and animals. One method used to detect these analytes is fluorescence microscopy. A variety of small-molecule fluorescent probes for the detection of NO, HNO, or mobile zinc have been developed and proven useful in studying the biochemistry of these species. Despite the value of these sensors, improved probes with greater selectivity and enhanced photophysical properties are needed to study the biological activity of inorganic molecules and ions, especially in live tissues and animals.

1.2 Small Molecule Fluorescent Sensors for Nitric Oxide, Nitroxyl, and Mobile Zinc

Small molecule fluorescent probes that exhibit a fluorescence enhancement (turn-on) response upon exposure to a particular species can be used to monitor NO, HNO, and zinc in live cells. A variety of different sensing mechanisms for each of these analytes have been developed.[33] One of the mechanisms commonly invoked in the design NO and HNO sensors relies on chromophoric ligands, the fluorescence of which is quenched upon binding of paramagnetic transition metals, such as Cu(II). Reaction of the metal complex with NO or HNO reduces the Cu(II) center to Cu(I), which results in a diamagnetic complex and restoration of the fluorescence of the probe.[34] The reduction potential of the bound copper ion can be tuned to alter the selectivity of the probe for either NO or HNO, based on the different reduction potentials of these two species.[35,36]

An example of an NO sensor based on this design principle is CuFL1 (Figure 1.1).[37] CuFL1 is the first of a series of NO specific probes characterized by a fluorescein dye functionalized with an aminoquinoline Cu(II) binding site. NO induces the reduction of Cu(II) to Cu(I), with concomitant nitrosation of the aminoquinoline ligand, resulting in an ~16-fold fluorescent turn-on response.[38] Only a few HNO probes have been developed.[39,40,41,42,43,44] One example that is based on the copper reduction mechanism is CuBOT1 (Figure 1.1), a BODIPY-based fluorophore functionalized with a tripodal Cu(II) binding site. Upon addition of 100 equivalents of HNO, CuBOT1 shows an immediate ~8-fold fluorescence enhancement in cuvettes. CuBOT1, however, is also sensitive to thiols and displays a strong turn-on in HeLa cells upon addition of 200 equivalents of cysteine. [39,40]

A common approach for the development of mobile zinc sensors is to take advantage of photoinduced electron transfer (PET). For these probes, an electron rich metal-binding unit is attached to a fluorophore and, in the absence of the metal ion, PET quenches the fluorescence of the fluorophore. Binding of zinc alleviates PET and restores the fluorescence of the probe. A large class of zinc-specific probes based on this sensing mechanism has been developed. One example is ZP1 (Figure 1.1), the first of the Zinpyr probes, which are a family of sensors characterized by a fluorescein dye and an amine-based zinc binding unit. By changing the zinc binding site, the affinity of the sensor can be tuned and probes have been developed with zinc affinities ranging from pM to mM.[45]

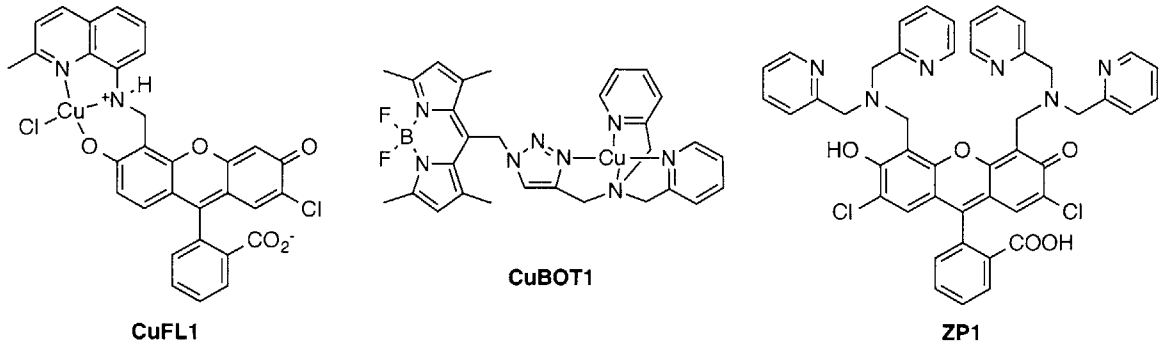

Figure 1.1. Selected small molecule fluorescent sensors for NO (CuFL1), HNO (CuBOT1), and Zn^{2+} (ZP1)

Although these probes have been useful, they can still be improved upon significantly in terms of their selectivity and photophysical properties. For example, many of the NO and HNO probes are sensitive to thiols and display a fluorescence response upon reaction with H_2S and cysteine.[39,40,42] Additionally, zinc probes that are based on the PET quenching mechanism are sensitive to pH and turn-on at low pH values.[45] It would be useful to develop probes not only with improved selectivity, but also with enhanced photophysical properties, such as greater brightness, quantum yields, or emission at longer wavelengths. Improving the photophysical properties would broaden the application of these probes in both tissues and live animals.

1.3 Tuning and Improving the Photophysical Properties of Sensors

An area of probe development is the creation of sensors that retain their selectivity but emit at longer wavelengths. Near-infrared (NIR) probes are useful for a variety of reasons, including reduced background emission, increased tissue penetration,[46] and ability to be used in multicolor microscopy experiments.[44,47,48] Several fluorophores have been developed that are bright, NIR emitters. These dyes include derivatives of cyanines,

squaraines, BODIPY, and dihydroxanthenes, among several others (Figure 1.2).[49,50,51] Each of these dyes contributes their own benefits and disadvantages, which should be carefully considered before being selected for incorporation into a new sensor.

For example, cyanine derivatives are typically bright and have been successfully used in the development of sensors of pH and reactive oxygen species. Squaraines are also bright, NIR emitters with narrow emission bands, but may display unwanted reactivity and tend to aggregate in aqueous solution. Only a few BODIPY derivatives emit in the NIR region and most emit in the yellow to deep red region of the electromagnetic spectrum. The xanthene structure is a common motif found in many fluorophores, including fluorescein and rhodamine and must be functionalized to obtain emission wavelengths in the NIR region. Additional properties that should be considered when selecting a fluorophore include its quantum yield, Stoke's shift, toxicity, and synthetic accessibility.[49,50]

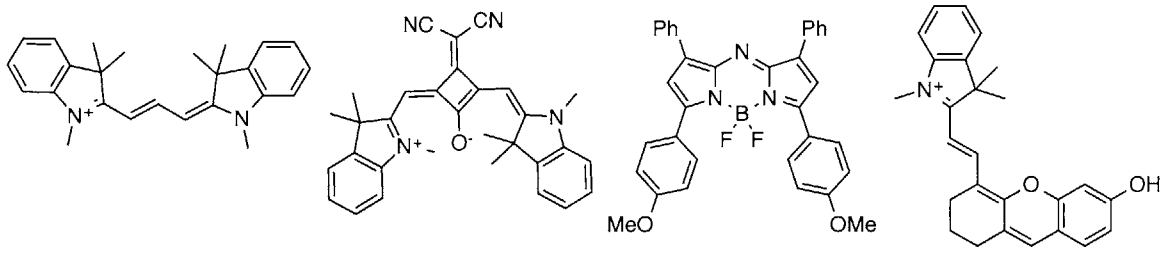

Figure 1.2. Selected NIR emitting dyes

1.4 Multicolor Microscopy

Sensors that emit in the NIR region can be used in combination with other probes or fluorescent proteins that emit at shorter wavelengths in multicolor microscopy experiments.[44,47,48,52,53] When used in combination with probes that selectively detect other analytes of biological interest, the interplay of two different species can be studied in real time. Recently, two red and NIR fluorescent sensors for the detection of calcium ion (Ca^{2+}) were reported and used in multicolor microscopy experiments.[47,53] The first of these probes is a red fluorescent sensor that localizes in the cytoplasm and was used in HeLa cells expressing cyan fluorescent protein in the nucleus and yellow fluorescent protein in the Golgi apparatus to image endogenous Ca^{2+} release upon histamine stimulation.[47] The second and NIR Ca^{2+} probe was also used to image Ca^{2+} release upon evocation of an action potential in neurons expressing green fluorescent protein (GFP).[53] A third recent example of multicolor imaging microscopy utilizes a Si-derivative of rhodamine conjugated to a drug to study the localization in cells expressing GFP.[52] These examples emphasize the utility of red and NIR fluorescent dyes and probes used in conjunction with fluorescent proteins to image specific analytes and intracellular location simultaneously.

Using these NIR and red probes along with other sensors that detect other analytes would allow for future studies that examine the relationship between multiple small molecule signaling molecules. One such example is the nitrosation of zinc thiolates, which may be a mechanism of endogenous release of mobile zinc.[54,55,56] Unlike NO,[57] HNO can react directly with thiols[14] and it may be able to stimulate the release of intracellular mobile zinc.

Efforts toward the development and characterization of red and NIR fluorescent probes for the detection of NO, HNO, and mobile zinc, as well as their implementation in multicolor imaging experiments, will be reported in the following chapters. Chapter 2 describes the synthesis and initial characterization of a NIR probe designed to detect NO. Based on what we learned through the development and characterization of this sensor, its structure was altered and the result was a fast and selective NIR HNO sensor.[58] The synthesis, characterization, and mechanistic studies of this sensor are discussed in Chapter 3. In addition, this probe was used in conjunction with ZP1 to study the interplay of HNO and release of mobile zinc in HeLa cells using multicolor microscopy. Chapter 4 presents an account of ongoing work toward the characterization and targeting of a red emitting, reaction-based, and pH insensitive zinc-specific probe.

Chapter 2 . Synthesis and Characterization of a Fluorescent Sensor with a Dihydrothioxanthene Fluorophore and a Quinoline Based Cu(II) Binding Site

2.1 Introduction

Nitric oxide (NO) is an important biological signaling molecule whose homeostasis is tightly regulated within the cellular environment.[34] To understand the circumstances that result in the up- or down-regulation of NO production in response to various stimuli, including other inorganic molecules or metals, it is desirable to develop a series of probes that emit at various visible and near-infrared (NIR) wavelengths. NO specific probes based on a copper-reduction mechanism have been developed. These sensors emit at a variety of wavelengths ranging from blue to red. [37,43,59,60,61,62,63]

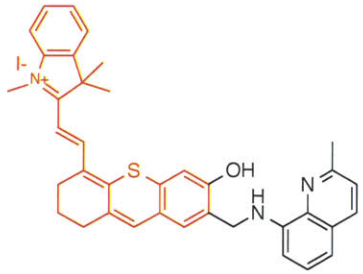

Figure 2.1. Structure of DTX-NO1. The portion highlighted in red is the DTX fluorophore and the portion shown in black is the quinoline-based Cu(II) binding site.

In an attempt to expand the range of emission wavelengths of these metal-based NO sensors, a NIR probe was designed and synthesized. This first-generation probe consists of a dihydrothioxanthene (DTX) fluorophore and a quinoline-based Cu(II) binding site, as shown in Figure 2.1, and is hereafter referred to as DTX-NO1. The DTX fluorophore is a derivative of the dihydroxanthene (DHX) chromophore, which displays excellent photophysical properties, biological compatibility, and synthetic accessibility.[64] Previous NO sensors, including the CuFL and BRNO series of probes, use a quinoline derivative as the basis for the Cu(II) binding site.[37,43] Given the success of this metal binding unit in the CuFL and BRNO series of probes, it was selected as the Cu(II) binding site for DTX-NO1.

2.2 Experimental Section

General Methods

All reactions were performed under a nitrogen atmosphere unless otherwise specified. Reagents were purchased from commercial sources and used as received. Solvents were purified and degassed by standard procedures. Nitric oxide was passed through an Ascarite column and a 6 ft coil containing silica gel at –78 °C to remove impurities and then collected and stored under nitrogen in a gas storage bulb. ^{1}H NMR spectra were acquired on a Varian Mercury 300 spectrometer. ^{1}H NMR chemical shifts are reported in ppm relative to $SiMe_4$ (δ = 0) and were referenced internally with respect to residual protons in the solvent (δ = 7.25 for $CDCl_3$ or δ = 3.31 for CD_3OD). Low-resolution mass spectra (LRMS) were acquired on an Agilent 1100 Series LC/MSD Trap spectrometer (LCMS), using electrospray ionization (ESI) or on an Agilent 5973 Network mass selective detector connected to an Agilent 689N Network GC-System using electron impact ionization (EI). IUPAC names of all compounds are provided and were determined using CS ChemBioDrawUltra 12.0.

For spectroscopic measurements, all solutions were prepared using de-ionized water with resistivity 18 mΩ/cm, obtained using a Milli-Q water system. All solvents were supplied by Aldrich and used as received. Piperazine-*N*,*N*'-bis(2-ethanesulfonic acid) (PIPES) and 99.999% KCl were purchased from Calbiochem, high purity 25% HCl, 45% KOH, and 50% NaOH were purchased from Aldrich. UV-Visible spectra were acquired using a Cary 50 spectrometer using quartz cuvettes from Starna (1 cm path length). Fluorescence spectra were acquired on a Photon Technology International fluorimeter. All measurements were conducted at 25 °C kept by circulating water baths.

Synthesis

*Synthesis of O-(4-Formyl-3-methoxyphenyl) Dimethylcarbamothioate (**1**).*

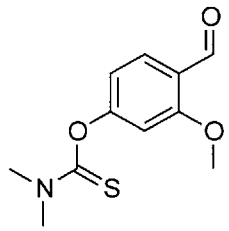

This compound was prepared according to a literature procedure.[65] Briefly, 4-hydroxy-2-methoxybenzaldehyde (2000 mg, 13.1 mmol) and DABCO (2950 mg, 26.3 mmol) were dissolved in dry DMF (20 mL). Dimethylthiocarbamoyl chloride (3250 mg, 26.3 mmol) was added and the mixture was stirred overnight at room temperature. The solution was poured onto ice and stored at 4 °C for 24 h. The precipitate was collected, washed with water, dissolved in CH_2Cl_2, dried with Na_2SO_4, filtered, and the solvent was evaporated under reduced pressure to give the product as a white solid (3.1 g, yield 98%). Mp: 109–129 °C. LRMS (ESI). Calcd for $[C_{11}H_{14}NO_3S]^+$: 240.3, found 240.1. ^{1}H NMR (300 MHz, $CDCl_3$): 3.36 (s, 3H), 3.46 (s, 3H), 3.92 (s, 3H), 6.73 (s, 1H), 6.74 (d, ^3J = 9 Hz), 7.86 (d, ^3J = 9 Hz, 1H), 10.40 (s, 1H).

*Synthesis of S-(4-Formyl-3-methoxyphenyl) Dimethylcarbamothioate (**2**).*

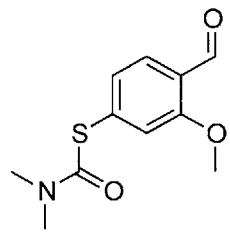

This compound was prepared according to a literature procedure.[65] Briefly, compound **1** (3100 mg, 12.9 mmol) was placed in a round bottom flask equipped with a reflux condenser. The compound was heated to 185 °C. After 4 h, the crude oil was cooled and purified by column chromatography (SiO_2; hexanes/EtOAc 7:3) to give the product (1700 mg, yield 55%). LRMS (ESI). Calcd for $[C_{11}H_{14}NO_3S]^+$: 240.3, found 240.1. ^{1}H NMR (300 MHz, $CDCl_3$): 3.11 (s, 6H), 3.94 (s, 3H), 7.14 (d, ^3J = 9 Hz, 1H), 7.20 (s, 1H), 7.80 (d, ^3J = 9 Hz, 1H), 10.44 (s, 1H).

Synthesis of S-(4-Formyl-3-hydroxyphenyl) Dimethylcarbamothioate (3).

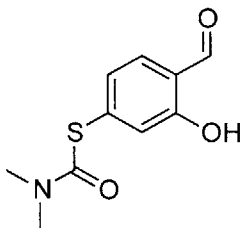

This compound was prepared according to a literature procedure.[65] Briefly, compound **2** (1700 mg, 7.11 mmol) was dissolved in CH_2Cl_2 (4.8 mL) and cooled to –10 °C. BBr_3 (1 M in CH_2Cl_2 (9.6 mL)) was slowly added while warming the mixture to room temperature. After 3 h, the reaction was quenched by pouring the solution into 40 mL of 1 M HCl in ice. The suspension was extracted with diethyl ether and the organic phase was washed with brine, dried with Na_2SO_4, filtered. The solvent was evaporated under reduced pressure to give the product as pale yellow needles (1190 mg, yield 74%). LRMS (ESI). Calcd for $[C_{10}H_{12}NO_3S]^+$: 226.3, found 226.0. Mp: 98–99 °C. ^{1}H NMR (300 MHz, $CDCl_3$): 3.06 (s, 6H), 7.14 (d, ^3J = 9 Hz, 1H), 7.20 (s, 1H), 11.01 (s, 1H).

Synthesis of 2-Methylquinolin-8-amine (4).

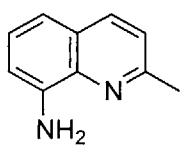

2-Methyl-8-nitroquinoline (2000 mg, 10.6 mmol) was dissolved in a mixture of EtOH/EtOAc (1:1 v/v, 10 mL) and Pd/C (200 mg) was added in one portion. The mixture was stirred for 48 h under an atmosphere of hydrogen. The suspension was filtered through Celite and the solvent was evaporated under reduced pressure to give the product as a brown solid (1100 mg, yield 66%). Mp: 64–66 °C. LRMS (EI). Calcd for $[C_{10}H_{10}N_2]$: 158, found 158. ^{1}H NMR (300 MHz, $CDCl_3$): 2.74 (s, 3H), 5.33 (bs, 2H), 6.91 (d, ^3J = 9 Hz, 1H), 7.11 (dd, ^3J = 9 Hz, ^3J = 1 Hz, 1H), 7.24 (d, ^3J = 3 Hz, 1H), 7.27 (d, ^3J = 3 Hz, 1H), 7.98 (d, ^3J = 9 Hz, 1H).

*Synthesis of O-(3-Hydroxy-4-(((2-methlyquinolin-8-yl)amino)methyl)phenyl) Dimethyl-carbamothioate (**5**).*

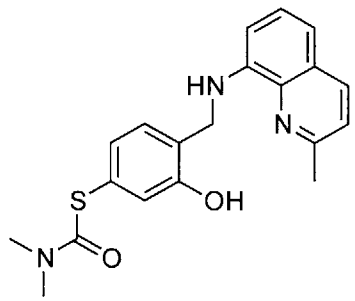

Compound **3** (500 mg, 2.22 mmol) and compound **4** (350 mg, 2.22 mmol) were dissolved in CH_3OH (24 mL). $NaBH(AcO)_3$ (418 mg, 6.66 mmol) was added in one portion and the mixture was stirred for 24 h. The solvent was evaporated under reduced pressure and the solid was redissolved in CH_2Cl_2 and washed with 10 mL of brine. The aqueous and organic phases were separated, the organic phase was dried with Na_2SO_4 and filtered, and the solvent was evaporated under reduced pressure. The crude oil was purified by column chromatography (Al_2O_3; CH_2Cl_2 to CH_2Cl_2/ CH_3OH 98:2) to give the product as a red-orange solid (790 mg, yield 97%). Mp: 76–82 °C. LRMS (ESI). Calcd for $[C_{20}H_{22}N_3O_2S]^+$: 368.5, found 368.1. ^{1}H NMR (300 MHz, $CDCl_3$): 2.70 (s, 3H), 3.06 (s, 6H), 4.57 (s, 2H), 6.88 (d, ^3J = 9, 1H), 7.03–7.05 (m, 2H), 7.18 (dd, ^3J = 6, ^3J = 3 Hz, 1H), 7.24–7.33 (m, 3H), 7.98 (d, ^3J = 9 Hz, 1H).

*Synthesis of 1,2,3,3-Tetramethyl-3H-indol-1-ium Iodide (**6**).*

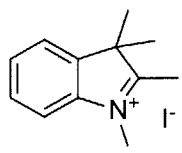

This compound was prepared according to a literature procedure.[66] Briefly, 2,3,3-trimethyl-3H-indole (3000 mg, 18.8 mmol) and methyl iodide (4011 mg, 28.3 mmol) were dissolved in toluene (20 mL) and heated to reflux. After 6 h, the suspension was cooled to room temperature, filtered, and the precipitated crystals were washed with toluene and diethyl ether to give a light purple

product (2220 mg, yield 39%). Mp: 250–264 °C. LRMS (ESI). Calcd for $[C_{12}H_{16}N]^+$: 174.3, found 174.0.

Synthesis of (E)-2-Chloro-3-(hydroxymethylene)cyclohex-1-enecarbaldehyde (7).

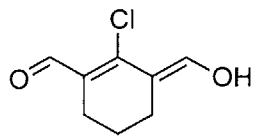

This compound was prepared according to a literature procedure.[67] Briefly, a mixture of DMF and CH_2Cl_2 (1:1 v/v, 40 mL) was cooled to 0 °C. $POCl_3$ (20 mL, 214.60 mmol) was added dropwise, followed by addition of cyclohexanone (5.3 mL, 50.9 mmol). The mixture was heated to reflux for 4 h, cooled to room temperature, poured onto ice-cold water, and stored at 4 °C overnight. The precipitate was filtered, washed with water, and dried under vacuum to give the product (6.8 g, yield 77%). LRMS (ESI). Calcd for $[C_8H_8ClO_2]^-$: 171.6, found 170.8.

*Synthesis of 2-((E)-2-((E)-2-Chloro-3-((E)-2-(1,3,3-trimethylindolin-2-ylidene)-ethylidene)cyclohex-1-en-1-yl)vinyl)-1,3,3-trimethyl-3H-indol-1-ium Iodide (**8**).*

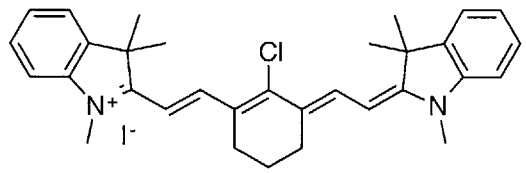

Compound **6** (631 mg, 3.65 mmol) and compound **7** (2220 mg, 7.30 mmol) were placed in a Schlenk flask equipped with a Dean-Stark trap and dissolved in a mixture of n-butanol/toluene (4:1 v/v, 30 mL). The mixture was heated to reflux. After 2 h, the solvent was evaporated under reduced pressure. The crude product was purified by column chromatography (SiO_2; CH_2Cl_2/ CH_3OH 99:1 to CH_2Cl_2/ CH_3OH 95:5). The dye was obtained as a green powder (1.80 g, yield 81%). Mp: 247–249 °C. LRMS (ESI). Calcd for $[C_{32}H_{36}ClN_2]^+$: 484.1, found 483.4.

^{1}H NMR (300 MHz, $CDCl_3$): 1.60 (s, 12H), 1.97 (m, 2H), 2.74–2.78 (m, 3H), 3.76 (s, 6H), 6.26 (d, ^3J = 15 Hz, 2H), 7.16–7.19 (m, 2H), 7.35–7.37 (m, 3H), 7.39–7.42 (m, 2H), 8.13 (d, ^3J = 12 Hz, 2H).

Synthesis of (E)-2-(2-(6-Hydroxy-7-(((2-methylquinolin-8-yl)amino)methyl)-2,3-dihydro-1H-thioxanthen-4-yl)vinyl)-1,3,3-trimethyl-3H-indol-1-ium Iodide (DTX-NO1).

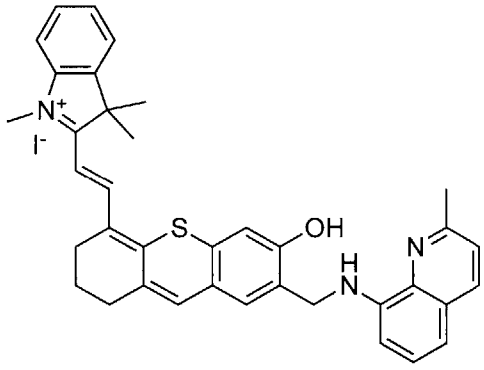

Compound **5** (100 mg, 0.272 mmol) was dissolved in CH_3OH (3 mL) under air atmosphere. KOH (230 mg, 4.09 mmol) was added in one portion and the mixture was heated to reflux. After 2 h, the KOH was neutralized with aqueous HCl and the solvent was evaporated under reduced pressure. The intermediate was isolated as the disulfide of compound **5** and mixed with dithiothreitol (DTT, 42 mg, 0.272 mmol) in DMF (2 mL). Et_3N (0.5 mL) was added and the mixture was stirred at room temperature for 30 min. Compound **8** (166 mg, 0.272 mmol) was added in DMF (1 mL) and the mixture was heated to 90 °C. After 1 h, the solvent was evaporated under reduced pressure and the crude product was purified using column chromatography (SiO_2; CH_2Cl_2/ CH_3OH 97:3) to give the sensor as a blue solid (~5 mg). LRMS (ESI). Calcd for $[C_{37}H_{36}N_3OS]^+$: 570.8, found 570.2. ^{1}H NMR (300 MHz, $CDCl_3$): 1.69 (s, 6H), 1.82–1.86 (m, 2H), 2.58 (m, 4H), 2.74 (s, 3H), 4.64 (s, 2H), 5.53 (d, ^3J = 12 Hz, 1H), 6.54 (d, ^3J = 9 Hz, 1H), 6.73–6.80 (m, 2H), 7.00 (m, 2H), 7.14 (s, 1H), 7.22 (m, 1H), 7.25 (s, 2H), 7.28 (s, 1 H), 7.41 (s, 1H), 7.62 (d, ^3J = 12 Hz, 1H), 7.96 (d, ^3J = 9 Hz, 1H).

Spectroscopic Methods and Anaerobic Sample Preparation

A 1.5 mM stock solution of ligand DTX-NO1 was prepared and stored at −20 °C in a 1 mL aliquot and thawed immediately before each experiment. The copper complex (CuDTX-NO1) was prepared by dissolving the ligand in 1 mL of DMSO, adding 1 equiv of $CuCl_2$, and stirring for 5 h. Extinction coefficients of the ligand and copper complex were determined using 5−15 μM solutions in aqueous buffer. Fluorescence quantum yields were determined using the same solutions (λ_{ex} = 715 nm). Fluorescence emission spectra were integrated from 725 to 900 nm. Quantum yields were referenced to sensor DTX1 (ϕ = 0.0089).*

Degassed aliquots of the stock solution of CuDTX-NO1 were brought into an anaerobic chamber under a nitrogen atmosphere (O_2 < 1 ppm) dedicated to work with aqueous solutions (hereafter called the "wet box"). Solutions containing 10 μM CuDTX-NO1 were prepared using 2 mL aqueous buffer (50 mM PIPES, 50 mM KCl, pH 7) in gastight cuvettes. NO gas was removed from the wet box in a gastight syringe and injected into the headspace of each gastight cuvette before measuring fluorescence.

2.3 Results and Discussion

Synthesis and Characterization of DTX-NO1

Sensor DTX-NO1 was synthesized by preparing the Cu(II) binding site and the fluorophore in parallel, followed by a ring-closing reaction to give the final sensor. The synthesis of the quinoline Cu(II) binding site began with 4-hydroxy-2-methoxybenzaldehyde, which was converted to **1** using dimethylthiocarbamoyl chloride

* P. Rivera-Fuentes and S.J. Lippard, *unpublished results.*

(DMTCC). Compound **1** was isomerized to **2** through a Newman-Kwart rearrangement, and **2** was subsequently demethylated using BBr_3 to give compound **3** (Scheme 2.1).[65]

Scheme 2.1. Synthesis of Compound **3**. Reagents and conditions: (a) DMTCC, DABCO, DMF, RT, 16 h, 98%, (b) 185 °C, 2 h, 55%, (c) BBr_3, CH_2Cl_2, –10 °C to RT, 3 h, 74%. DMTCC = dimethylthiocarbamoyl chloride, DABCO = 1,4-diazabicyclo[2.2.2]octane.

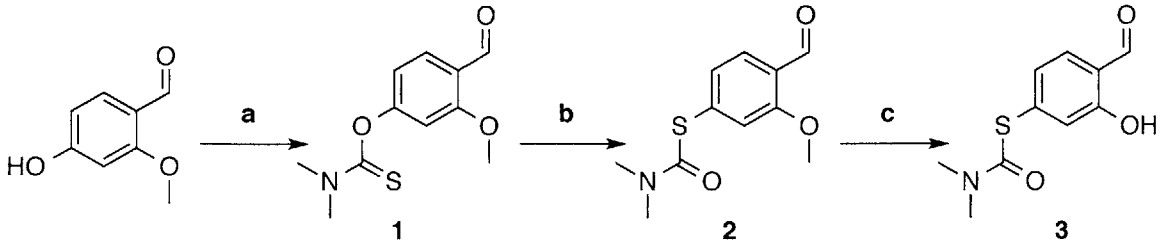

To complete the Cu(II) binding site, 2-methyl-8-nitroquinoline was hydrogenated to give compound **4**. Using a reductive amination, intermediates **3** and **4** were coupled to form compound **5** (Scheme 2.2),[63] completing the synthesis of the Cu(II) binding site.

Scheme 2.2. Synthesis of Compound **5**. Reagents and conditions: (a) H_2, Pd/C, EtOH/EtOAc, RT, 24 h, 66%, (b) Compound **3**, $NaBH_3CN$, CH_3OH, RT, 40 h, 97%.

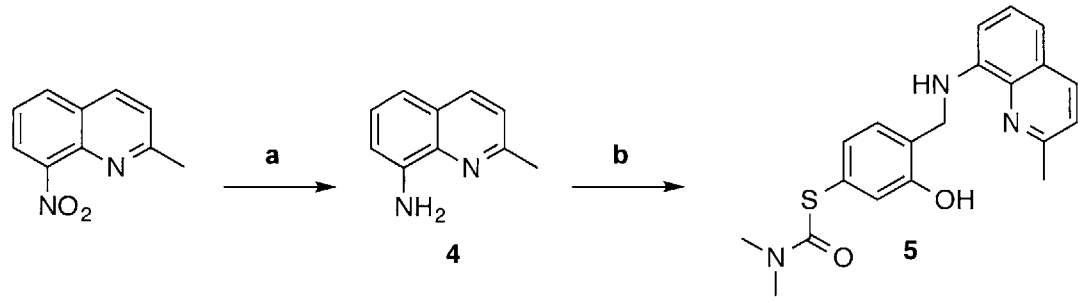

The basis of the fluorophore is a heptamethine cyanine dye. To prepare this dye, indolenine was first methylated to give **6**.[66] Compound **7** was obtained via Vilsmeier formylation of cyclohexanone.[67] Compounds **6** and **7** were reacted to give the heptamethine cyanine dye **8** (Scheme 2.3).[68]

Scheme 2.3. Synthesis of Compound **8**. Reagents and conditions: (a) CH_3I, toluene, reflux, 2 h, 39%, (b) $POCl_3$, DMF, $CHCl_3$, 60 °C, 2 h, 77%, (c) BuOH/toluene, reflux, 2 h, 81%.

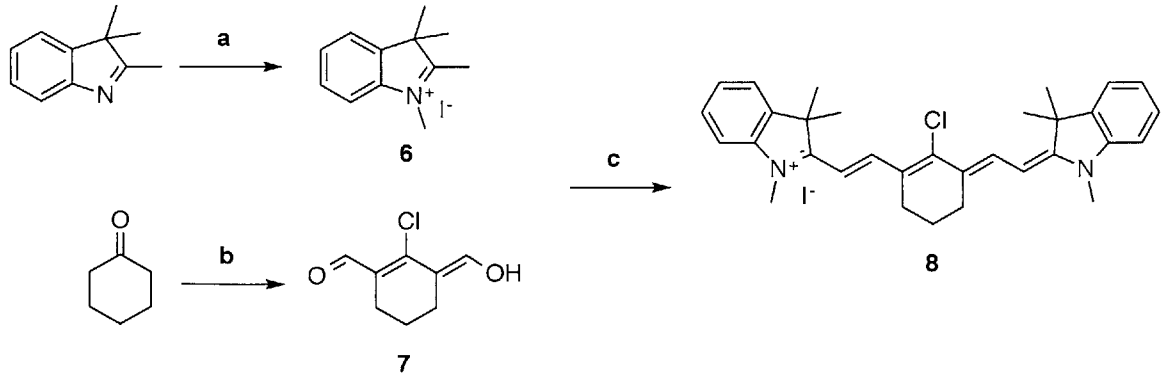

To complete the synthesis, the protecting group on the sulfur of **5** was removed using potassium hydroxide to give the disulfide of **5**.[65] This intermediate was reduced *in situ* using dithiothreitol (DTT) and reacted with **8** to give the final sensor, DTX-NO1 (Scheme 2.4).

Scheme 2.4. Synthesis of DTX-NO1. Reagents and conditions: (a) KOH, CH_3OH, reflux, 2 h, then DTT, Et_3N, DMF, 80 °C, 3 h. DTT = dithiothreitol.

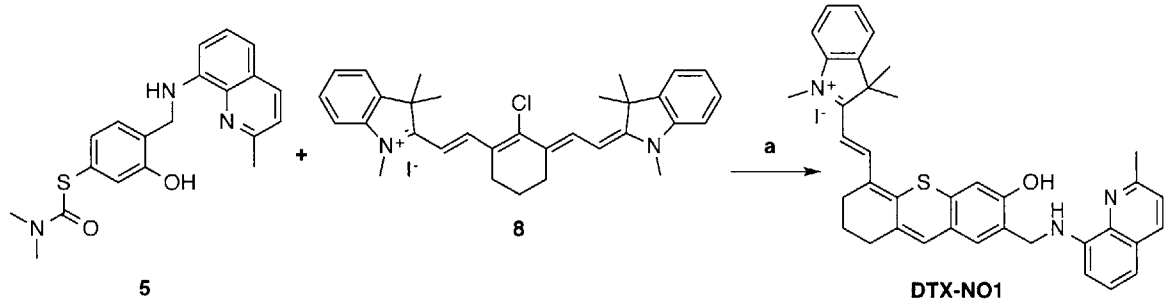

The photophysical properties of both DTX-NO1 and its Cu(II) complex (CuDTX-NO1) were measured in aqueous buffer (50 mM PIPES, 100 mM KCl, pH 7) and are summarized in Table 2.1. Both DTX-NO1 and CuDTX-NO1 displayed broad absorption spectra that extend into the NIR region and, upon exciting at 715 nm, showed a maximum fluorescence emission at 758 nm (Figure 2.2). Unexpectedly, the brightness ($\varepsilon\phi$) of both DTX-NO1 and CuDTX-NO1 was very low: 3 and 2 $M^{-1}cm^{-1}$, respectively. These values are more than three orders of magnitude lower than that of Indocyanine

Green (1.1 x10^3 M^{-1} cm^{-1}), a NIR fluorophore used for in vivo imaging.[69] Both DTX-NO1 and CuDTX-NO1 exhibited effectively quenched fluorescence emission in aqueous buffer.

Table 2.1. Summary of Photophysical Properties of DTX-NO1 and CuDTX-NO1

	absorption: λ_{max} (nm); ε ($cm^{-1}M^{-1}$)	emission: λ_{max} (nm); ϕ
DTX-NO1	758; 2.3(1) x10^3	763; 0.0013(3)
CuDTX-NO1	692; 5.9(3) x 10^3	763; 0.00040(3)

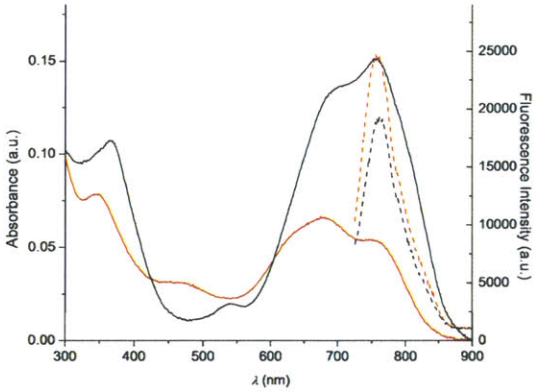

Figure 2.2. Photophysical properties of DTX-NO1. Fluorescence (dotted lines) and absorbance (solid lines) spectra of DTX-NO1 (red lines) and CuDTX-NO1 (black lines) in aqueous buffer (50 mM PIPES, 100 mM KCl, pH 7); λ_{ex}= 715 nm.

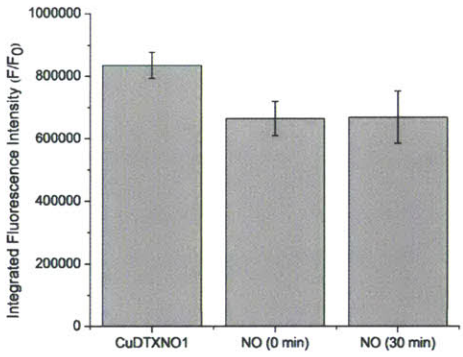

Figure 2.3. CuDTX-NO1 reactivity toward NO. Integrated fluorescence intensity (725–900 nm) of 10 μM CuDTX-NO1 in aqueous buffer (50 mM PIPES, 100 μM KCl, pH 7) and 0 and 30 min after addition of 5000 equiv of NO gas; λ_{ex} = 715 nm.

Despite these unfavorable photophysical properties, the reactivity of CuDTX-NO1 toward NO was investigated. Upon addition of excess NO gas, no significant change in fluorescence intensity was observed (Figure 2.3). This observation suggests that either there is no reaction between NO and CuDTX-NO1 or the change in fluorescence intensity cannot be detected because of the already quenched fluorescence of the ligand.

Self-Quenching of DTX-NO1

The low fluorescent intensity of DTX-NO1 was investigated using DFT calculations (B3LYP/6-31G*). These calculations revealed the presence of a quinoline-centered molecular orbital located between the π and π* fluorophore-based orbital. These results indicate that electron transfer may occur from a fluorophore-centered π* orbital to a quinoline centered π* orbital, which can decay to the ground state via a non-radiative pathway (Figure 2.4).

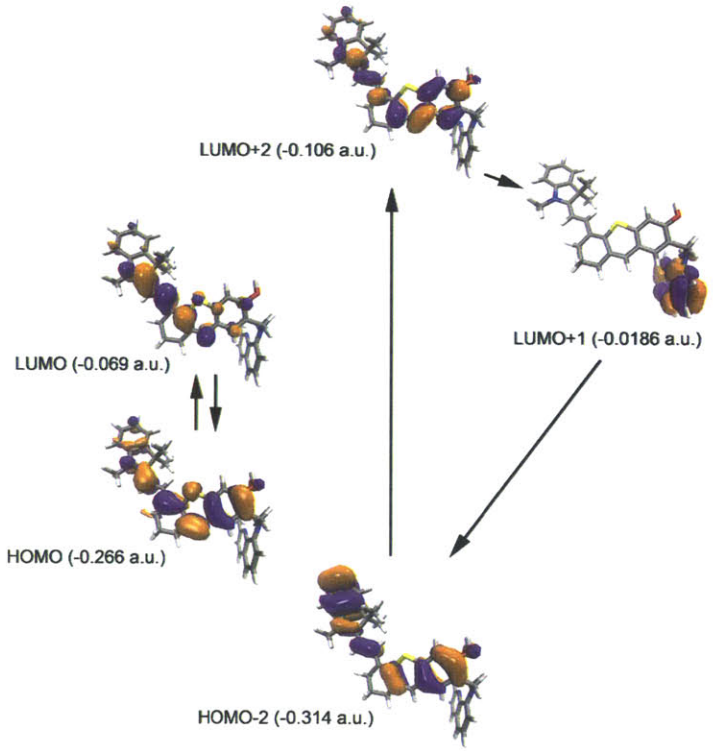

Figure 2.4. DFT calculations for DTX-NO1. Results of DFT calculations reveal a quinoline-centered molecular orbital in between π and π* fluorophore-based orbitals.

2.4 Conclusions

Probe DTX-NO1 is not suitable for use in biological systems because of its low brightness and it was not further characterized. We hypothesize that changing the Cu(II) binding site would alleviate the self-quenching of the fluorophore. A second-generation probe, which lacks a heteroaromatic binding site, is proposed. This new probe comprises a cyclam Cu(II) binding site, which would eliminate the non-radiative decay pathway that may be occurring in DTX-NO1. The synthesis, characterization, and implementation of this probe will be discussed in Chapter 3.

Chapter 3 . Synthesis, Characterization, and Implementation of a Near-Infrared Fluorescent Sensor for Detection of Nitroxyl (HNO)

3.1 Introduction

Nitroxyl (HNO), the one electron reduced and protonated form of nitric oxide (NO) may be an important biological signaling molecule, but its biochemistry has remained underexplored because of the lack of methods to visualize it directly in live cells, tissues, and animals. This chapter describes the design, synthesis, and use of a fluorescent probe that detects HNO both in cuvettes and in live cells. As discussed in Chapter 2, the heteroaromatic Cu(II) binding site quenches the fluorescence of the NIR fluorophore. To eliminate this self-quenching, an alternative structure is proposed. This new probe comprises a dihydroxanthene (DHX) fluorophore and a Cu(II) cyclam binding site (Figure 3.1) and is hereafter referred to as DHX1. The DHX fluorophore was chosen for its photophysical properties and biological compatibility.[64] The Cu(II) cyclam binding site was selected because it is not a heteroaromatic ring system and because Cu(II) cyclam complexes react slowly with H_2S and glutathione.[70] Several of the available NO and HNO sensors based on a copper reduction mechanism are susceptible to reducing thiols and display a turn-on response in the presence of these analytes.[39,40,42] It would be valuable to develop a copper-based sensor that is selective for HNO or NO over intracellular thiols.

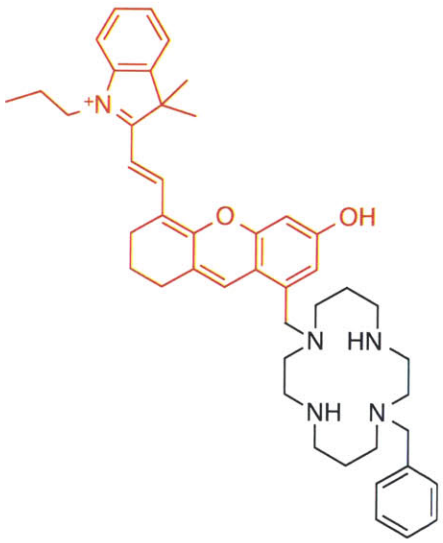

Figure 3.1. Structure of DHX1. The portion highlighted in red is the DTX fluorophore and the portion shown in black is the quinoline-based Cu(II) binding site.

Altering the Cu(II) binding site can change the reduction potential of the bound metal. The BRNO series of probes comprise a benzoresorufin-based fluorophore and various Cu(II) binding sites. The reduction potentials of these copper complexes range from 10 mV to 150 mV (vs. Fc/Fc^+).[43] The reduction potential of NO/HNO is –0.11 V (vs NHE)[35] and that of NO^+/NO is 1.52 V (vs. NHE),[36] suggesting that tuning the reduction potential of the bound copper can alter the selectivity of the probe.

3.2 Experimental Section

General Methods

All reactions were performed under a nitrogen atmosphere unless otherwise specified. ZP1 was prepared as previously described.[71] Reagents, solvents, and NO gas were purchased or prepared as outlined in Chapter 2. NMR spectra were acquired on a Varian Inova-500 or a Varian Mercury-300 instrument. ^{1}H NMR chemical shifts are reported in ppm relative to $SiMe_4$ (δ = 0) and were referenced internally with respect to residual protons in the solvent (δ = 3.31 for CD_3OD or δ = 2.50 for DMSO-d_6). ^{13}C NMR chemical shifts are reported in ppm relative to $SiMe_4$ (δ = 0) and were referenced internally with respect to solvent signal (δ = 39.51 for DMSO-d_6). ^{19}F NMR chemical shifts are reported in ppm relative to $CFCl_3$ (δ = 0) and were referenced internally with respect to 2,2,2-trifluoroethanol (δ = –77.03). Low-resolution mass spectra (LRMS) were acquired on an Agilent 1100 Series LC/MSD Trap spectrometer (LCMS), using electrospray ionization (ESI). High-resolution mass spectrometry (HR-ESI-MS) was conducted by staff at the MIT Department of Chemistry Instrumentation Facility on a Bruker Daltonics APEXIV 4.7 T FT-ICR-MS instrument. Semipreparative HPLC

separations were carried out on an Agilent 1200 HPLC instrument with a multiwavelength detector and automated fraction collector using a C18 reverse stationary phase (Zorbax-SB C18, 5 μm, 9.5 × 250 mm) and a mobile phase composed of two solvents (A: 0.1% (v/v) trifluoroacetic acid (TFA) in H_2O; B: 0.1% (v/v) TFA in CH_3CN). Specific purification protocols are described below for each compound. IUPAC names of all compounds are provided and were determined using CS ChemBioDrawUltra 12.0.

Synthesis

*Synthesis of (E)-2-(2-(6-Hydroxymethyl)-2,3-dihydro-1H-xanthen-4-yl)vinyl)-3,3-dimethyl-1-propyl-3H-indol-1-ium Iodide (**1**).*

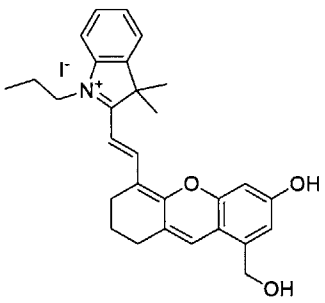

A solution of dye IR780 (300 mg, 0.45 mmol) in dry DMF (5 mL) was added to 5-(hydroxymethyl)benzene-1,3-diol (63 mg, 0.45 mmol). Triethylamine (0.6 mL, 4.49 mmol) was added, and the mixture was stirred at 110 °C for 30 min. The solvent was evaporated under reduced pressure and the solid was purified by column chromatography (SiO_2; CH_2Cl_2/CH_3OH 9:1) to give the product as a dark blue solid (195 mg, yield 76%). LRMS (ESI). Calcd for $[C_{29}H_{32}NO_3]^+$: 442.2, found 442.2. ^1H NMR (300 MHz, CD_3OD): 1.04 (t, ^3J = 7.4 Hz, 3H), 1.80 (s, 6H), 1.89–1.96 (m, 4H), 2.69–2.82 (m, 4H), 4.26 (t, ^3J = 7.2 Hz), 4.79 (s, 2H), 6.40 (d, ^3J = 14.7 Hz, 1H), 6.74 (d, ^4J = 2 Hz, 1H), 6.91 (d, ^4J = 2 Hz, 1H), 7.36–7.41 (m, 1H), 7.45–7.49 (m, 2H), 7.60–7.63 (m, 1H), 7.70 (s, 1H), 8.69 (d, ^3J = 14.5 Hz, 1H).

*Synthesis of (E)-2-(2-(8-(Chloromethyl)-6-hydroxy-2,3-dihydro-1H-xanthen-4-yl)vinyl)-3,3-dimethyl-1-propyl-3H-indol-ium Iodide (**2**).*

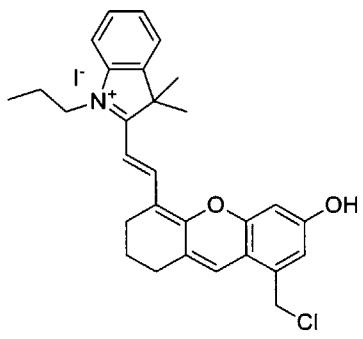

Thionyl chloride (75 μL, 1.03 mmol) and dry pyridine (83 μL, 1.03 mmol) were dissolved in dry CH_2Cl_2 (1 mL) and cooled to 0 °C. Compound **1** (195 mg, 0.34 mmol) was dissolved in dry CH_2Cl_2 (1 mL) and dry DMF (0.1 mL) and added slowly to the mixture of pyridine and thionyl chloride. After 30 min, H_2O (0.1 mL) was added and the mixture was dried with Na_2SO_4 and filtered. The solvent was evaporated under reduced pressure. The dark blue solid was dissolved in CH_2Cl_2/CH_3OH (9:1) and filtered through a plug of SiO_2 eluting with CH_2Cl_2/CH_3OH (9:1, 200 mL). The solvent was evaporated, and the crude product was used immediately. LRMS (ESI). Calcd for $[C_{29}H_{31}ClNO_2]^+$: 460.2, found 460.1.

*Synthesis of (E)-2-(2-(8-((1,4,8,11-Tetraazacyclotetradecan-1-yl)-methyl)-6-hydroxy-2,3-dihydro-1H-xanthen-4-yl)vinyl)-3,3-dimeth-yl-1-propyl-3H-indol-1-ium Trifluoroacetate (**3**).*

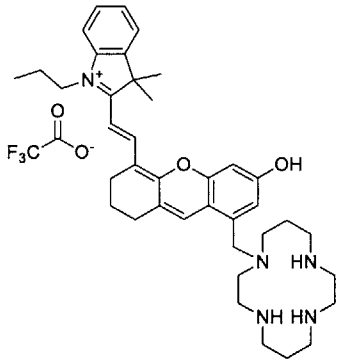

A solution of crude compound **2** in dry CH_3CN (3 mL) was added to 1,4,8,11-tetraazacyclotetradecane (cyclam, 136 mg, 0.68 mmol). Diisopropylethylamine (0.12 mL, 0.68 mmol) was added and the mixture was heated to reflux. After 30 min, the solvent was evaporated and the residue was purified by RP-HPLC according to the following protocol: constant flow rate 3 mL min^{-1}; isocratic flow 2% B, 0–5 min; gradient, 35–95% B,

10–25 min. The product was collected between 16.5–16.8 min. All equivalent fractions recovered from independent runs were combined and lyophilized to dryness to yield the TFA salt of compound **3** (46 mg, 18% over two steps). Mp: 110–120 °C. HR-ESI-MS. Calcd for $[C_{39}H_{54}N_5O_2]^+$: 624.4273, found: 624.4259. ^{1}H NMR (500 MHz, DMSO-d_6): 0.96 (t, ^3J = 7.4 Hz, 3H), 1.72 (s, 7H), 1.81 (m, 7H), 2.67 (m, 10H), 3.10 (m, 10H), 3.80 (s, 2H), 4.35 (t, ^3J = 7.1 Hz, 2H), 6.53 (d, ^3J = 15 Hz, 1H), 6.92 (m, 1H), 7.42, (t, ^3J = 7.7 Hz, 1H), 7.51 (t, ^3J = 8.3 Hz, 1H), 7.66 (d, ^3J = 8.0 Hz, 1H), 7.72 (d, ^3J = 7.7 Hz, 2H), 8.55 (d, ^3J = 15 Hz, 1H). ^{13}C NMR (125 MHz, DMSO-d_6): 11.08, 20.10, 20.92, 23.60, 27.59, 28.55, 40.44, 45.95, 49.56, 50.24, 101.59, 103.73, 113.12, 113.38, 113.71, 115.75, 115.96, 118.11, 120.48, 122.76, 125.85, 126.85, 127.96, 128.97, 136.75, 141.65, 141.88, 144.50, 154.73, 158.13, 158.42, 158.65, 158.90, 160.62, 161.12, 177.01. ^{19}F NMR (282 MHz, CD_3OD): –75.31.

*Synthesis of (E)-2-(2-(8-((8-Benzyl-1,4,8,11-tetraazacyclotetradecan-1-yl)methyl)-6-hydroxy-2,3-dihydro-1H-xanthen-4-yl)vinyl)-3,3-dimethyl-1-propyl-3H-indol-1-ium Trifluoroacetate (**DHX1**).*

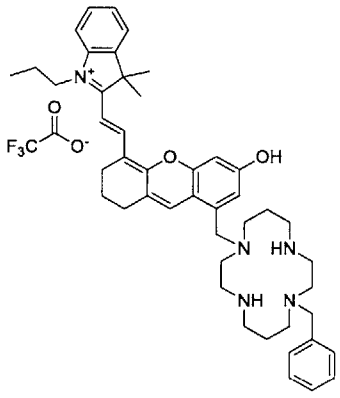

A solution of compound **3** (46 mg, 0.06 mmol) in CH_3CN (3 mL) and (bromomethyl)benzene (4 µL, 0.03 mmol) were combined. Diisopropylethylamine (22 µL, 0.12 mmol) was added and the reaction mixture was stirred at room temperature for 2 h. The solvent was evaporated and the product was purified by RP-HPLC according to the following protocol: constant flow rate 3 mL min^{-1}; isocratic flow 2% B, 0–5 min; gradient,

35–95% B, 10–25 min. The product was collected between 18.1–18.5 min. All equivalent fractions recovered from independent runs were combined and lyophilized to dryness to yield the TFA salt of compound DHX1 (14.2 mg, 28%). Mp: 115–120 °C. HR-ESI-MS. Calcd for $[C_{46}H_{60}N_5O_2]^+$: 714.4742, found: 714.4758. ^{1}H NMR (500 MHz, DMSO-d_6): 0.97 (t, ^3J = 7 Hz, 3H), 1.72 (s, 6H), 1.80 (m, 6H), 2.06 (m, 2H), 2.66 (m, 3H), 2.72 (m, 5H), 3.14 (m, 8H), 3.83 (s, 3H), 4.35 (t, ^3J = 7 Hz, 2H), 6.52 (d, ^3J = 15 Hz, 1H), 6.91 (m, 1H), 7.00 (m, 1H), 7.40 (m, 6H), 7.50 (t, ^3J = 7, 1H), 7.66 (d, ^3J = 5 Hz, 1H), 7.72 (m, 2H), 8.54 (d, ^3J = 15 Hz, 1H).^{13}C NMR (125 MHz, DMSO-d_6): 11.09, 20.09, 20.89, 23.60, 27.57, 27.62, 28.50, 40.43, 45.91, 50.20, 50.24, 53.71, 57.10, 101.27, 103.55, 113.07, 113.32, 113.52, 113.69, 113.85, 115.69, 116.11, 118.06, 120.42, 122.76, 125.63, 126.78, 128.29, 128.44, 128.93, 130.06, 130.37, 131.40, 141.64, 141.85, 144.41, 154.66, 158.02, 158.04, 158.51, 158.81, 160.80, 161.29,176.87. ^{19}F NMR (282 MHz, CD_3OD): –75.18.

Spectroscopic Methods and Anaerobic Sample Preparation

Spectroscopy techniques were described in Chapter 2. Stock solutions of compound **3** and ligand DHX1 in DMSO were prepared in the 1–8 mM range and stored at –20 °C in 1 mL aliquots and thawed immediately before each experiment. The copper complexes were prepared by dissolving the ligand in 1 mL of CH_3OH, adding 1 equiv of $CuCl_2$, and stirring overnight. The solvent was evaporated, and the solid was redissolved in 1 mL DMSO and stored at –20 °C. All spectroscopic measurements were conducted in aqueous buffer containing 50 mM PIPES (pH 7.0) and 100 mM KCl, with the exception of those performed in CH_3OH and at varying pH values. Extinction coefficients of the ligands and

sensors were determined by using 1–3 μM solutions in aqueous buffer. Fluorescence quantum yields were determined using the same solutions, λ_{ex} = 650 nm. Fluorescence emission spectra were integrated from 660 to 900 nm. Quantum yields were referenced to IR780, which has a reported quantum yield of 0.076 in CH_3OH, λ_{ex} = 725 nm.[72]

Degassed aliquots of the stock solutions of each sensor were brought into the wet box. Solutions containing 5 μM Cu-**3** and 2 μM CuDHX1 were prepared using 2 mL of either degassed aqueous buffer or CH_3OH in gastight cuvettes. Angeli's salt ($Na_2N_2O_3$, Cayman Chemical) was used as the source of HNO, because it decomposes rapidly ($t_{1/2}$ = 3 min) at pH 7 to produce HNO and $NaNO_2$.[73] Solutions of Angeli's salt (4 mM) were prepared in the wet box in degassed 10 mM NaOH (2 mL) and brought out of the wet box in a gastight syringe. NO gas was removed from the wet box in a gastight syringe and injected into the headspace of each gastight cuvette before measuring fluorescence.

Analyte Selectivity Studies

Selectivity of the sensor toward biologically relevant analytes was determined by comparing the fluorescence emission spectra of a 2 μM solution of CuDHX1 in aqueous buffer at pH 7, before and after treatment with 100 equiv of $CaCl_2$, $MgCl_2$, NaCl, $ZnCl_2$, KNO_3, $NaNO_2$, KO_2, H_2O_2, NaClO, sodium ascorbate, NaONOO, L-(+)-cysteine hydrochloride, gluthathione, methionine, Na_2S, or Angeli's salt. NO gas (5000 equiv) and 100 mL of 10 mM NaOH (solvent of Angeli's salt solutions) were also tested. In each case, the response was quantified by integrating the emission intensity from 660 to 900 nm and normalized to that of 2 μM CuDHX1 in aqueous buffer. For the NO and HNO selectivity studies, the samples were prepared anaerobically. For the NO, HNO, and

Na_2S studies, fluorescence spectra were acquired every 1 min for 10 min. For the remaining analytes, the fluorescence spectra were recorded at 0, 5, and 10 min. To determine the effect of pH on the fluorescence emission of CuDHX1, 2 μM solutions of CuDHX1 were prepared anaerobically in aqueous buffer (either 50 mM MES, 100 mM KCl; pH 4 and 5 or 50 mM PIPES, 100 mM KCl; pH 6, 7, and 8), and fluorescence spectra were recorded before and after addition of 100 equiv of Angeli's salt.

Cyclic Voltammetry

All electrochemistry measurements were carried out by Dr. Timothy C. Johnstone. Cyclic voltammograms were measured in a three-electrode cell with a 2.0 mm diameter glassy carbon working electrode, a platinum auxiliary electrode, and Ag/Ag^+ pseudoreference electrode in acetonitrile. The solvent contained 0.1 M *n*-Bu_4NPF_6 as the supporting electrolyte. The measurements were performed at room temperature with a VersaSTAT3 potentiostat from Princeton Applied Research operated with V3 studio software. Measurements were carried out at a scan rate of 200 mV s^{-1} on quiescent solutions that had been sparged with N_2 for 5 min. All data were referenced to the Fc/Fc^+ couple as an internal standard.

Electron Paramagnetic Resonance Spectroscopy

All EPR spectra were measured by Ms. Alexandria D. Liang. Low temperature X-band EPR spectra (77 K, 9 GHz) were collected with a Bruker EMS spectrometer equipped with an ER 4199HS cavity and a Gunn diode microwave source. EPR samples were prepared anaerobically. Solid DHX1 and **3** were brought into a glovebox. 0.8 equiv of

$Cu(MeCN)_4BF_4$ were added to 400 μM DHX1 or **3** in 350 μL CH_3OH, stirred overnight, and brought out of the glovebox in sealed EPR tubes. Angeli's salt (100 equiv) was prepared in 10 mM NaOH anaerobically and brought out of the wet box in a gastight syringe. For the NO reactivity test, degassed aliquots from the stock solution of CuDHX1 and Cu-**3** were brought into a wet box. Solutions containing 400 μM CuDHX1 or Cu-**3** were prepared in 350 μL of degassed CH_3OH and brought out of the wet box in sealed EPR tubes. NO gas was taken out of the wet box in a gastight syringe and injected into the headspace of the EPR tube.

Mammalian Cell Culture, Staining, and Imaging Procedures

HeLa cells were cultured in Dulbecco's modified Eagle medium (DMEM; Cellgro, MediaTec, Inc.), supplemented with 10% fetal bovine serum (FBS; HyClone), 1% penicillin-streptomycin, 1% sodium pyruvate, and 1% L-glutamine. The cells were grown to 90% confluence at 37 °C with 5% CO_2 before being passed and plated onto poly-D-lysine-coated plates 48 h before imaging. All cells were used between passage number 5 and 15. Imaging was conducted when plates reached 50–70% confluence. The growth medium was replaced with phosphate-buffered saline (PBS) containing 5 μM CuDHX1 and 3 μM Hoechst 33528 dye, and the cells were incubated for 15 min. Cells were rinsed with PBS (2 × 2 mL) followed by addition of fresh PBS (2 mL) and mounted on the microscope. For cell imaging experiments with ZP1, the growth medium was replaced with dye-free DMEM containing 5 μM ZP1, 3 μM Hoechst 33528 dye, and the cells were incubated for 1 h. Cells were rinsed with PBS (2 × 2 mL) before addition of fresh PBS

containing 5 μM CuDHX1 and incubated for 15 min. Cells were rinsed with PBS (2 × 2 mL), followed by addition of fresh PBS (2 mL) and mounted on the microscope.

Imaging experiments were performed using a Zeiss Axiovert 200 M inverted epifluorescence microscope equipped with an EM-CCD digital camera (Hamamatsu) and a MS200 XY Piezo Z stage (Applied Scientific Instruments). The light source was an X-Cite 120 metal-halide lamp (EXFO), and the fluorescence images were obtained using an oil-immersion objective at 63× or 100× magnification. The filters sets used are defined as blue: excitation G 365 nm, beamsplitter FT 395 nm, emission BP 445/50 nm; green: excitation BP 470/40 nm, beamsplitter FT 495 nm, emission 525/50 nm; NIR: excitation HQ 650/45 nm, beamsplitter Q 680 nm, emission HQ 710/50 nm. The microscope was operated using Volocity software (Perkin-Elmer).

The exposure times for acquisition of fluorescence images were kept constant for each series of images at each channel. To measure analyte induced fluorescence changes, a solution of Angeli's salt or Na_2S was added to the plate on the microscope stage to reach a concentration of 1.5 mM, and images were taken immediately after addition and after 5 min. Mobilization of intracellular zinc was induced by treating the cells with 3 mM Angeli's salt, and the released Zn^{2+} was chelated by bathing the cells in a solution of fresh PBS containing 50 μM *N*,*N*,*N*′,*N*′-tetrakis(2-pyridylmethyl)ethylenediamine (TPEN). Quantification of fluorescence intensity was performed using ImageJ (version 1.45, NIH). The whole cell was selected as the region of interest, and the integrated fluorescence from the background region was subtracted from the cell body region.

3.3 Results and Discussion

Synthesis and Characterization of DHX1 and CuDHX1

The synthesis of ligand DHX1 started with a reaction between 5-(hydroxymethyl)benzene-1,2-diol and IR780, a commercially available heptamethine cynanine dye, to give compound **1**. The isolated alcohol was converted into compound **2** using thionyl chloride. The chloride was used immediately to give compound **3** via a nucleophilic substitution reaction with cyclam. Compound **3** was subsequently alkylated using benzyl bromide to give ligand DHX1 (Scheme 3.1). Both ligand **3** and DHX1 were purified using RP-HPLC and isolated with a trifluoroacetate as the counter ion, as determined by ^{19}F NMR. The copper complexes of **3** and DHX1 were prepared using $CuCl_2$. ESI-MS measurements showed that a trifluoroacetate ligand is bound to complexes Cu-**3** and CuDHX1.

Scheme 3.1. Synthesis of **3** and DHX1. Reagents and conditions: (a) Et_3N, DMF, 110 °C, 20 min, 78%; (b) $SOCl_2$, pyridine, CH_2Cl_2, DMF, 0 °C, 30 min; (c) Cyclam, DIPEA, CH_3CN, reflux, 30 min, 18% (over steps b and c); (d) Benzyl bromide, DIPEA, CH_3CN, 25 °C, 2 h, 28%. Counterions are omitted for clarity. DIPEA = diisopropylethylamine.

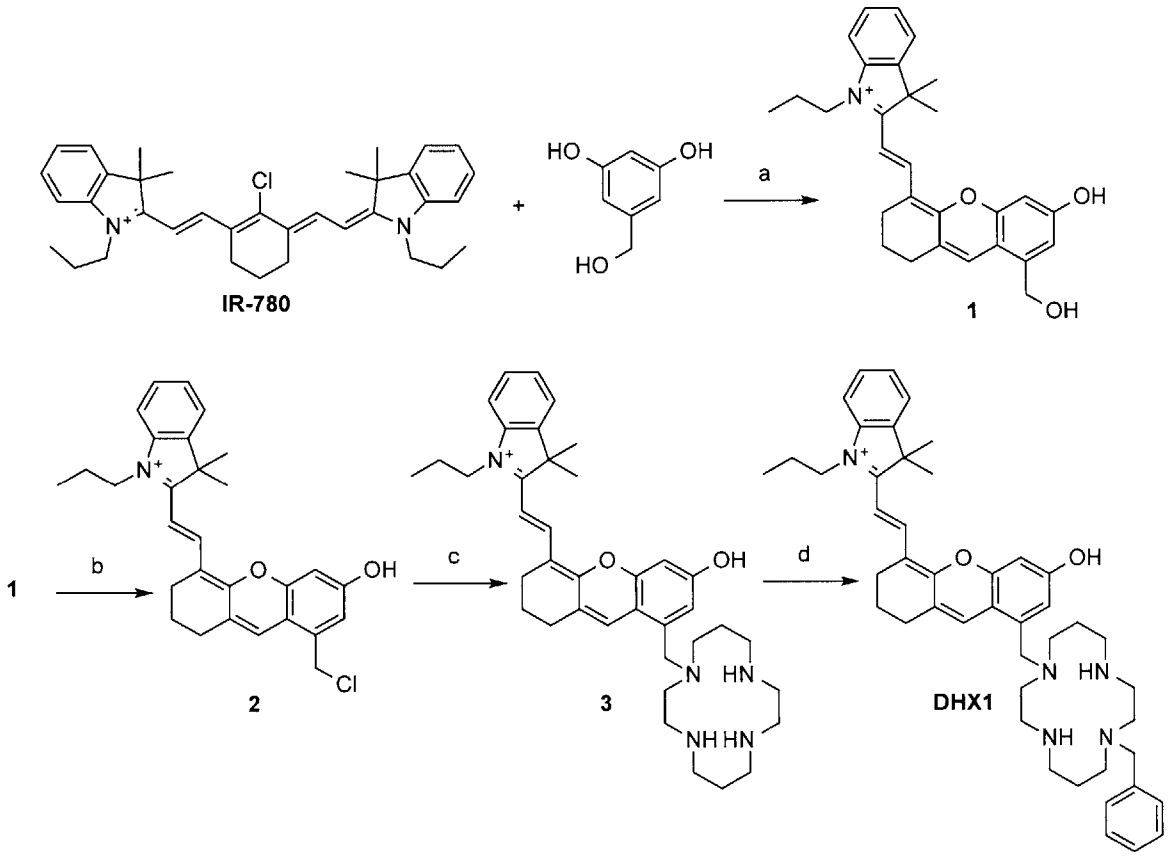

The photophysical properties of **3**, Cu-**3**, DHX1, and CuDHX1 were measured in aqueous buffer (50 mM PIPES, 100 mM KCl, pH 7) and are summarized in Table 3.1. The brightness ($\varepsilon\phi$) of both **3** and DHX1 are within the same order of magnitude, 1593 and 1104, respectively. These values indicate that **3** and DHX1 would be suitable for in vivo imaging, as they display $\varepsilon\phi$ values similar to that of Indocyanine Green.[74] Additionally, the $\varepsilon\phi$ values these ligands are several orders of magnitude larger than that of DTX-NO1 (Chapter 2). Replacing the quinoline binding site with a cyclam significantly increases the quantum yield of the ligand. Upon binding of paramagnetic Cu(II), the quantum yields of Cu-**3** and CuDHX1 are approximately one order of

magnitude lower than that of their respective ligands. Additionally, the absorption spectra for both **3** and DHX1 and their resulting copper complexes are broad and extend into the NIR region (Figure 3.2). Exciting at 650 nm gives a maximum in fluorescence intensity at 715 nm for each ligand and copper complex (Figure 3.2).

Table 3.1. Photophysical Properties of 3, Cu-3, DHX1, and CuDHX1

	absorption: λ_{max} (nm); ε ($cm^{-1}M^{-1}$)		**emission: λ_{max} (nm); ϕ**	
	ligand	Cu complex	ligand	Cu complex
3	693; 2.7(1) x10^4	693; 3.3(2) x 10^4	715; 0.059(2)	715; 0.0050(4)
DHX1	693; 2.3(1) x10^4	693; 2.9(1) x10^4	715; 0.048(3)	715; 0.0027(1)

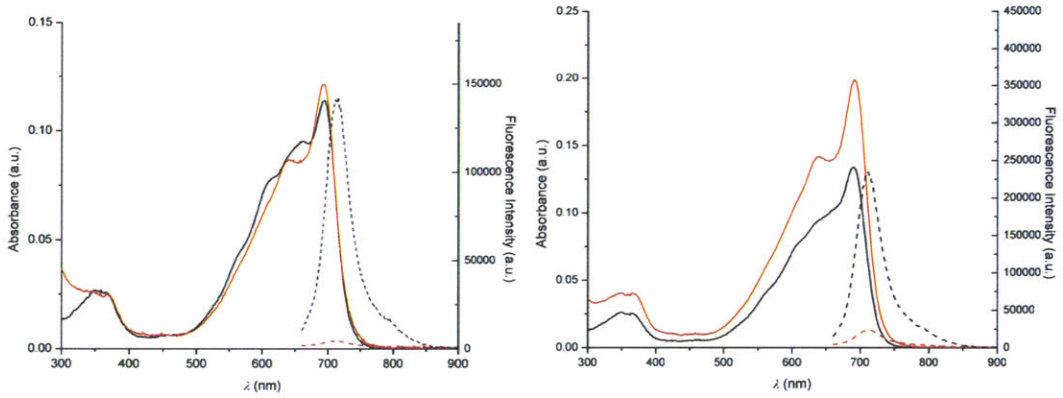

Figure 3.2. Photophysical properties of DHX1 and **3**. Fluorescence (dotted lines) and absorbance (solid lines) spectra of DHX1 (left, black lines), CuDHX1 (left, red lines), **3** (right, black lines), and Cu-**3** (right, red lines) in aqueous buffer (50 mM PIPES, 100 mM KCl, pH 7), λ_{ex} = 650 nm.

The reactivity of Cu-**3** and CuDHX1 toward HNO and NO was measured in aqueous buffer. To ensure reactivity with HNO or NO and not an oxidation product of these analytes, samples were prepared anaerobically. For the NO reactivity test, NO gas was injected directly into the headspace of each cuvette and the fluorescence turn-on was measured. For the HNO reactivity test, Angeli's salt was used as the source of HNO. Angeli's salt ($Na_2N_2O_3$) decomposes rapidly at pH 7 to generate nitrite and HNO.[73] Angeli's salt was prepared anaerobically in degassed 10 mM NaOH in order to slow its decomposition prior to addition to each sample. Upon addition of excess NO gas, both

CuDHX1 and Cu-**3** showed no change in fluorescence intensity (Figure 3.3). Upon addition of 100 equiv of Angeli's salt, Cu-**3** showed an ~3-fold increase in fluorescence intensity and CuDHX1 displayed an ~5-fold increase in fluorescence intensity (Figure 3.3).

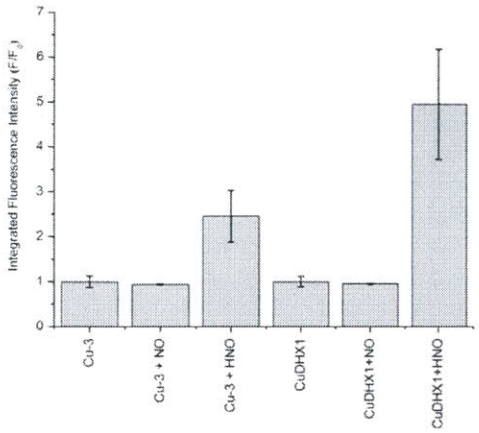

Figure 3.3. Cu-**3** and CuDHX1 reactivity toward HNO, NO. Fluorescence spectra of 5 μM Cu-**3** and 2 μM CuDHX1 (black dashed line) in aqueous buffer (50 mM PIPES, 100 mM KCl, pH 7) and 2 min after the addition of 100 equiv of Angeli's salt or 5000 equiv NO gas; λ_{ex}: 650 nm.

Given the ability of Angeli's salt to induce a larger fluorescence response in CuDHX1, compared to Cu-**3**, CuDHX1 was selected for further analysis. The reactivity of CuDHX1 toward Angeli's salt was first studied. CuDHX1 displayed a maximum increase in fluorescence intensity 2 minutes after addition of 100 equiv of Angeli's salt, and the fluorescence intensity slowly decreased over time (Figure 3.4). Moreover, addition of Angeli's salt did not restore completely the fluorescence of the ligand. Treatment of ligand DHX1 with 100 equiv of Angeli's salt induced a decrease in emission intensity (Figure 3.4). This result indicates that either Angeli's salt or one of its decomposition products reacts with ligand DHX1, causing a decrease in its fluorescence emission. We did not investigate further which product of Angeli's salt may be responsible for this reactivity or how it may be reacting with ligand DHX1.

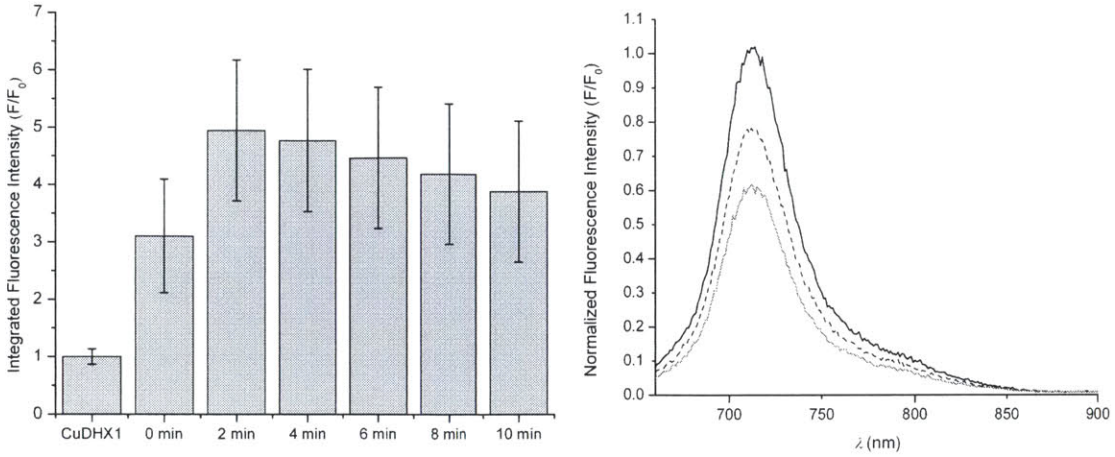

Figure 3.4. Reactivity of CuDHX1 and ligand DHX1 toward HNO (left) Time-dependent normalized integrated (660–900 nm) fluorescence intensity of 2 μM CuDHX1 in aqueous buffer (50 mM PIPES, 100 mM KCl, pH 7) after addition of 100 equiv of Angeli's salt. λ_{ex}: 650 nm. (right) Time-dependent fluorescence spectra of 2 μM DHX1 (black solid line) in aqueous buffer (50 mM PIPES, 100 mM KCl, pH 7) and after addition of 100 equiv of Angeli's salt (0 min: black dotted line; 10 min: grey solid line). λ_{ex}: 650 nm.

The HNO donor Angeli's salt was prepared in basic aqueous solution. To verify that HNO is responsible for the fluorescence turn-on observed for CuDHX1, the sensor was treated with 100 equiv $NaNO_2$ and 100 μL of 10 mM NaOH. No fluorescence turn-on was observed upon addition of either of these analytes after 10 minutes (Figure 3.5), proving that CuDHX1 does display a fluorescence enhancement upon reaction with HNO.

For CuDHX1 to have applications in live cells, it must be able to detect HNO selectively over biologically relevant metals and other reactive oxygen and nitrogen species. CuDHX1 showed no fluorescence turn-on upon addition of 100 equiv of $CaCl_2$, $MgCl_2$, NaCl, $ZnCl_2$, KNO_3, H_2O_2, NaClO, sodium ascorbate, NaONOO, cysteine, GSH, or methionine (Figure 3.5). The only analyte tested that induced a turn-on response in CuDHX1 was H_2S. It should be noted, however, that the turn-on with H_2S was slower and less intense than that induced with HNO (Figure 3.5).

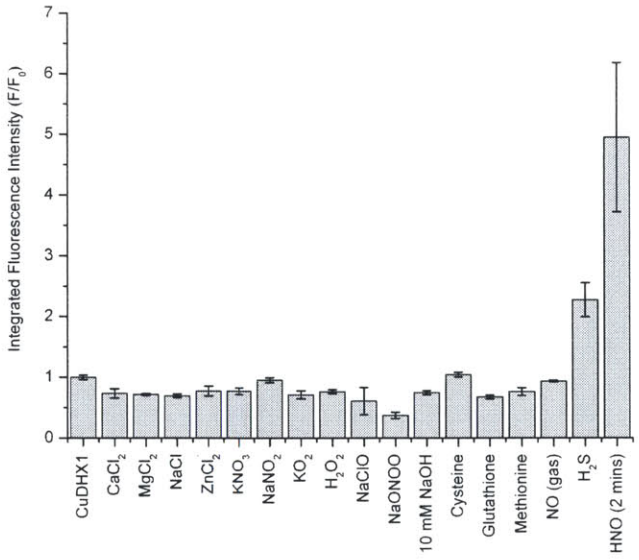

Figure 3.5. Analyte selectivity studies of CuDHX1. Normalized integrated fluorescence intensity (660–900 nm) of 2 mM CuDHX1 in aqueous buffer (50 mM PIPES, 100 mM KCl, pH 7) and 10 min after addition of 100 equiv of the analyte or 2 min after the addition of HNO. λ_{ex}: 650 nm.

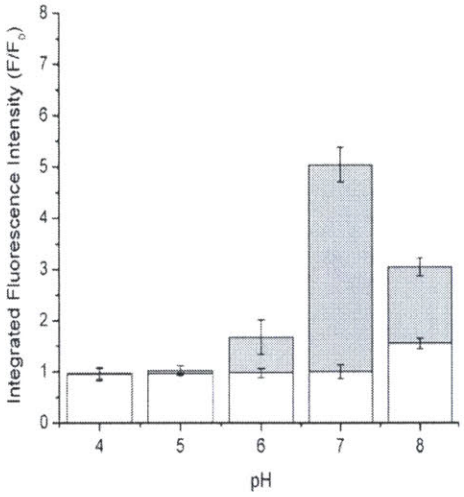

Figure 3.6. CuDHX1 turn-on response at varying pH. Normalized integrated (660–900 nm) fluorescence intensity of 2 μM CuDHX1 in aqueous buffer (0.1 M MES, 100 mM KCl; pH 4 and 5 or 50 mM PIPES, 100 mM KCl; pH 6, 7, and 8) before (white bars) and after (grey bars) addition of 100 equiv of Angeli's salt. The intensities were normalized with respect to 2 μM CuDHX1 at pH 7 before addition of Angeli's salt. λ_{ex}: 650 nm.

Additionally, the turn-on response of CuDHX1 at varying pH was measured. Changes in pH did not induce a fluorescence response in CuDHX1 (Figure 3.6). At low pH however, a blue shift and quenching of fluorescence was observed, most likely due to the protonation of the phenolic alcohol of the fluorophore.[73] These results indicate that changes in intracellular pH will not induce turn-on. The maximum fluorescence enhancement in response to addition of Angeli's salt occurred at pH 7, but small increases in fluorescence intensity were observed at pH 6 and 8 (Figure 3.6).

Sensing Mechanism of CuDHX1

Mechanistic studies were carried out to understand why CuDHX1 detects HNO selectively over NO, and why CuDHX1 displays a greater fluorescence turn-on compared to Cu-**3**. This investigation included cyclic voltammetry, EPR spectroscopy, and ESI-MS experiments.

The selectivity of Cu-**3** and CuDHX1 for HNO over NO can be explained using cyclic voltammetry. The voltammagram of CuDHX1 and Cu-**3** showed quasi-reversible Cu(II)/Cu(I) reductions with potentials summarized in Table 3.2. Comparison of these reduction potentials to those of the NO/HNO and NO^+/NO pairs revealed that CuDHX1 and Cu-**3** are thermodynamically able to reduce HNO, but not NO.

Table 3.2. Reduction Potentials for CuDHX1 and Cu-3

Reduction Event	Reduction Potential
Cu(II)/Cu(I) for CuDHX1	370 mV (vs Fc/Fc^+); 1.01 V (vs NHE)
Cu(II)/Cu(I) for Cu-**3**	325 mV(vs Fc/Fc^+); 0.96 V (vs NHE)
NO/HNO	-0.11 V (vs NHE)[35]
NO^+/NO	1.52 V (vs NHE)[36]

X-band EPR spectroscopy was used to investigate the sensing mechanisms of CuDHX1 and Cu-**3**. Solutions of the complexes Cu-**3** and CuDHX1 were prepared anaerobically. Prior to the addition of any analyte, the EPR spectra at 77 K of Cu-**3** and CuDHX1 were very similar and revealed a Cu(II) signal characteristic of a rhombic geometry. Upon addition of NO gas, no noticeable change in the EPR spectra of CuDHX1 was observed, confirming that NO does not reduce the Cu(II) bound to CuDHX1 (Figure 3.7).

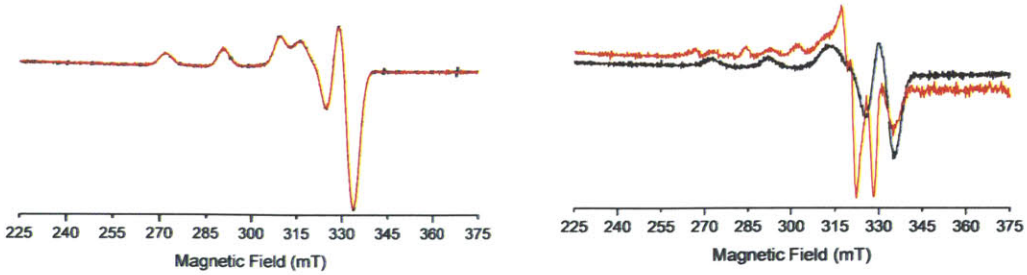

Figure 3.7. X-band EPR spectrum of Cu-**3**. X-band EPR spectra of 400 μM Cu-**3** in CH_3OH. Cu-**3** before (black line) and after addition of 100 equiv of Angeli's salt (red line). Collection parameters: temperature, 77 K; modulation amplitude, 20 G; microwave power, 0.2 mW at 9.23 GHz.

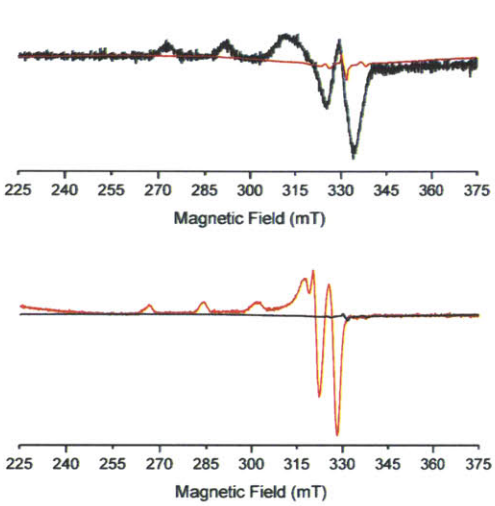

Figure 3.8. X-band EPR spectra of CuDHX1. X-band EPR spectra of 400 μM CuDHX1 in CH_3OH. Top: CuDHX1 before (black line) and after addition of 5000 equiv of NO (red line). Middle: CuDHX1 (left) before (black line) and after (red line) addition of 100 equiv of Angeli's salt. Bottom: CuDHX1 (left) after reduction by HNO (black line) and after reoxidation by air (red line). Collection parameters: temperature, 77 K; modulation amplitude, 20 G; microwave power, 0.2 mW at 9.23 GHz.

In a separate experiment, CuDHX1 was treated with 100 equiv of Angeli's salt, which led to disappearance of the Cu(II) signal, confirming reduction of Cu(II) to Cu(I). Upon reoxidation with air, the Cu(II) signal reappeared as a spectrum characteristic of a more axially symmetric geometry (Figure 3.7). In the case of complex Cu-**3**, addition of Angeli's salt did not abolish the Cu(II) signal. Instead, we observed a trace similar to that of the reoxidized species observed for CuDHX1 (Figure 3.8). These results suggest that if HNO reduces the Cu(II) center in Cu-**3**, it is immediately reoxidized, even under strict anaerobic conditions. The nature of the species responsible for the reoxidation of Cu(I) in Cu-**3** was not further investigated.

ESI-MS studies revealed that reaction of CuDHX1 with HNO induces dissociation of copper. Under the same reaction conditions, significant amounts of Cu-**3**

complex are detected, suggesting that this complex is more stable toward reduction-induced dissociation. It appears that the Cu-**3** complex is more prone to re-oxidation and that the copper remains bound after reaction with HNO and this may help explain the differences in fluorescence turn-on between Cu-**3** and CuDHX1.

Live Cell and Multicolor/Multianalyte Imaging

The ability of CuDHX1 to detect HNO in live cells was assessed using HeLa cells, which were incubated with 5 μM CuDHX1 and 3 μM Hoechst stain for 15 minutes in PBS buffer. Imaging was performed in PBS buffer because experiments in DMEM resulted in no fluorescence turn-on, presumably because Angeli's salt can react with cysteine or other components of DMEM.[75]

Prior to addition of Angeli's salt, only faint fluorescence was detected in the NIR channel. Five minutes after the addition of 1.5 mM Angeli's salt, a ~3-fold fluorescence enhancement was observed in the NIR channel (Figure 3.9).

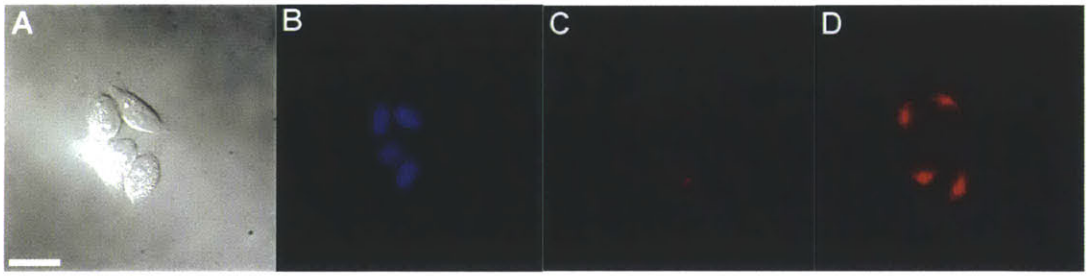

Figure 3.9. Turn-on response of CuDHX1 in HeLa cells. Fluorescence microscopy images of cells incubated with CuDHX1 in PBS before and after addition of Angeli's salt: (A) Differential interference contrast (DIC) image; (B) blue channel showing nuclei; (C) NIR channel before addition of Angeli's salt; and (D) NIR channel 5 min after treatment with 1.5 mM Angeli's salt. Scale bar = 25 μm.

The ability of CuDHX1 to detect HNO selectively over H_2S, the only analyte tested in cuvettes that promoted some fluorescence enhancement of CuDHX1, in live

cells was also assessed. Before treatment of the cells with H_2S, the NIR channel showed only faint fluorescence. Ten minutes after the addition of 1.5 mM Na_2S, only a slight turn-on in the NIR channel was observed. Upon subsequent addition of 1.5 mM Angeli's salt, a strong fluorescence enhancement was observed in the NIR channel (Figure 3.10). These results indicate that CuDHX1 can be used within the complex cellular environment to detect HNO, even in the presence of excess H_2S.

Figure 3.10. Selectivity of CuDHX1 for HNO over H_2S in HeLa cells. Selectivity of CuDHX1 in HeLa cells for HNO over H_2S. (A) DIC image, (B) NIR channel before treatment with 1.5 mM Na_2S, (C) NIR channel 10 min after treatment with 1.5 mM Na_2S, (D) NIR channel 10 min treatment with 1.5 mM Angeli's salt. Cells were incubated with 5 μM CuDHX1 in PBS. Scale bar = 25 μm.

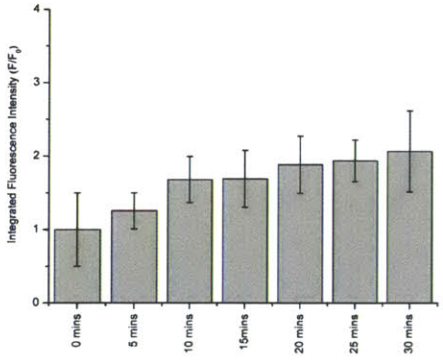

Figure 3.11 Turn-On of CuDHX1 in HeLa cells Time-dependent increase in integrated fluorescence intensity (NIR channel) of HeLa cells incubated with 5 μM CuDHX1 in PBS buffer.

It should be noted that in the absence of exogenously applied HNO, CuDHX1 showed a slight increase in fluorescence intensity over time in live cells. This turn-on, however, is much slower and less intense compared to the fluorescence enhancement observed upon addition of Angeli's salt (Figure 3.11).

NIR sensors are useful in that they can be used in multicolor imaging

microscopy experiments in combination with other sensors that emit at shorter wavelengths and detect other biologically relevant analytes. Using CuDHX1 and ZP1, a green, zinc-specific fluorescent sensor, the interplay between HNO and mobile zinc was investigated. As mentioned in Chapter 1, nitrosation of zinc thiolates can cause the release of mobile zinc.[54,55,56] Here, we investigated the ability of HNO to affect the levels of intracellular mobile zinc.

HeLa cells were co-incubated with both ZP1 and CuDHX1. Prior to addition of HNO, both the green and NIR fluorescent channels showed only faint fluorescence (Figure 3.12, Panels D and G). Upon addition of 3 mM Angeli's salt, both the green and NIR channels showed increased fluorescence intensity (Figure 3.12, Panels E and H). This result indicates that HNO has entered the cell and that mobile zinc has been simultaneously released. Upon addition of TPEN, an intracellular chelator, the fluorescence in the green channel decreased, confirming that the fluorescence response of ZP1 was a consequence of the release of mobile zinc (Figure 3.12, Panel F). No change in the NIR channel was observed upon addition of TPEN (Figure 3.12, Panel I).

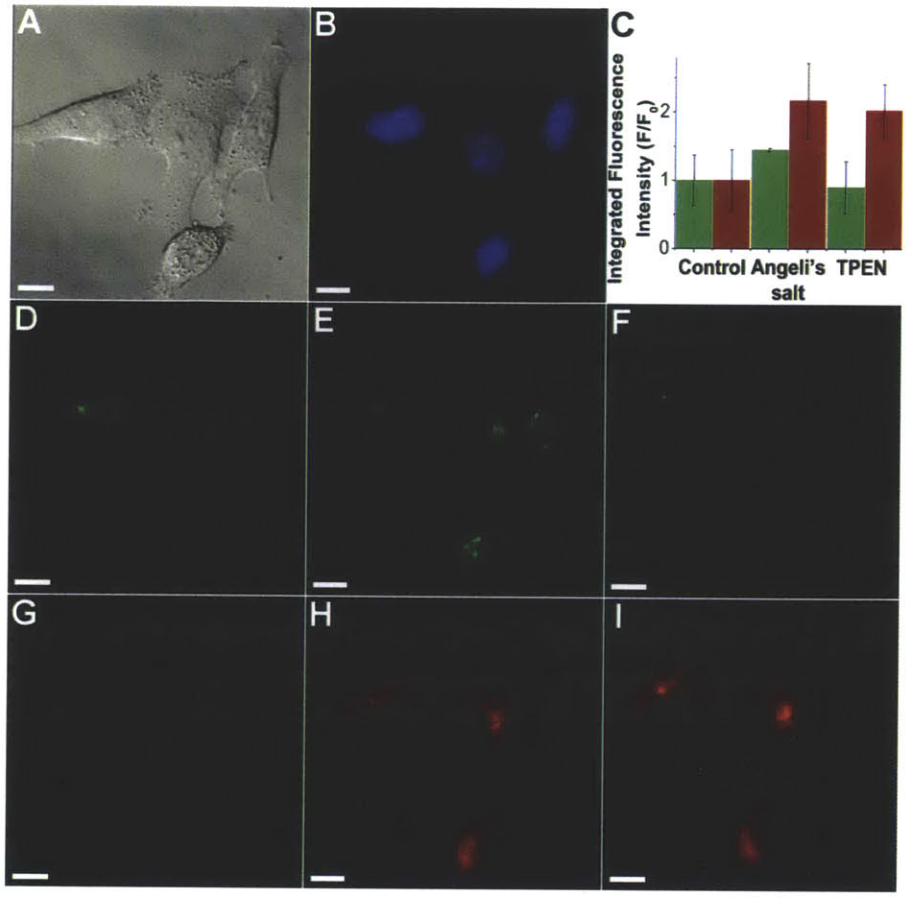

Figure 3.12. Multicolor/Multianalyte imaging of HNO and mobile zinc. (A) DIC image; (B) blue channel showing nuclei; (C) quantification of the fluorescence intensity in the green and NIR channels; (D) green channel before addition of Angeli's salt; (E) green channel after addition of Angeli's salt; (F) green channel after addition of TPEN; (G) NIR channel before addition of Angeli's salt; (H) NIR channel after addition of Angeli's salt; and (I) NIR channel after addition of TPEN. Scale bar =10 μm.

Angeli's salt decomposes to give HNO and $NaNO_2$ at pH 7.[73] To verify that HNO was responsible for the release of mobile zinc, $NaNO_2$ in 10 mM NaOH (solvent of Angeli's salt solution) was added to the cells. No change in the green channel was observed (Figure 3.13), confirming that HNO was responsible for the release of mobile zinc.

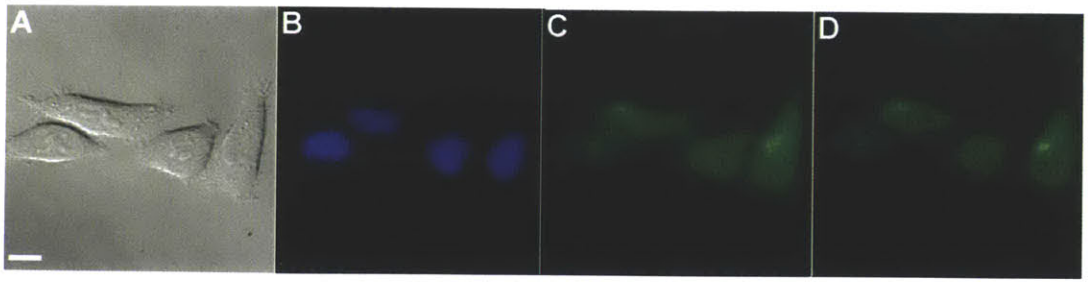

Figure 3.13. Zinc induced fluorescence selectivity over $NaNO_2$ and NaOH. Zinc induced fluorescence selectivity over $NaNO_2$ and NaOH. HeLa cells containing ZP1 and treated with 3 mM $NaNO_2$ in aqueous 10 mM NaOH. (A) DIC image, (B) Blue channel showing nuclei, (C) Green channel before addition of $NaNO_2$, (D) Green channel 20 min after treatment with 3 mM $NaNO_2$ in aqueous 10 mM NaOH. Scale bar = 10 μm.

3.4 Conclusions

A NIR fluorescent sensor for the detection of HNO was synthesized, characterized, and implemented in live cells to study the interplay between HNO and mobile zinc. CuDHX1 is fast and selective for HNO over intracellular thiols, metals, and other reactive oxygen and nitrogen species. The sensing mechanism of CuDHX1 relies on the selective reduction of Cu(II) to Cu(I) and dissociation of the metal complex. Using this sensor, we studied the relationship between HNO and the intracellular levels of mobile zinc. Given the advantages of this sensor over previously developed probes, future work with CuDHX1 could include its intracellular targeting and use to detect endogenous production of HNO in response to varying stimuli.

Chapter 4 . Characterization and Targeting of a Red Zinc Sensor

4.1 Introduction

Zinc (II) is an important signaling metal ion in biology and is tightly regulated within the cell. Fluorescent probes have been useful in studying the levels of intracellular mobile zinc,[34] but the available sensors have limitations in terms of their short emission wavelength and pH sensitivity. A recently developed probe, SpiroZin1, overcomes these two specific shortcomings.[76] SpiroZin1 is a red, reaction-based zinc probe that comprises a dipicolylamine (DPA) zinc binding arm and a spirobenzopyran that undergoes a zinc-induced ring-opening reaction to produce a red emissive cyanine (Figure 4.1).

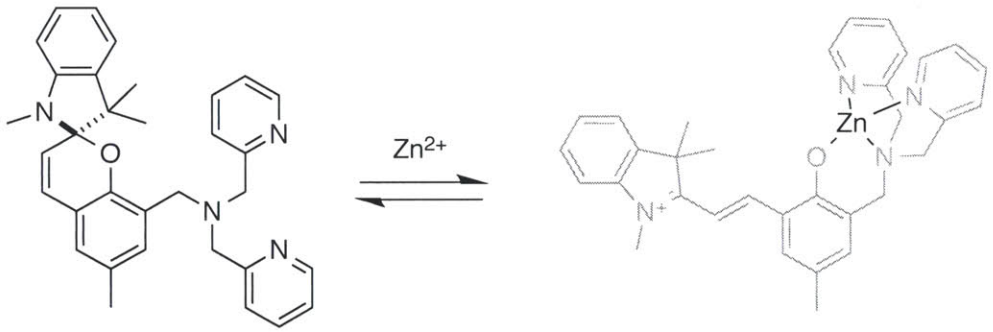

Figure 4.1. Sensing mechanism of SpiroZin1.

SpiroZin1 binds Zn^{2+} with picomolar affinity, which may lead to binding of zinc bound to proteins and not only ions in mobile pools. To tune the binding affinity of the SpiroZin scaffold and broaden its application in live cells, a series of sensors with modified zinc binding units were prepared. The chelating units are methyl(pyrazine)picolylamine (Figure 4.2, SpiroZin2), methyl(pentafluorophenyl)-picolylamine (Figure 4.2, SpiroZin3),[†] and methyl(thiophene)picolylamine (Figure 4.2,

[†] SpiroZin3 was synthesized and characterized by P. Rivera-Fuentes. This compound will not be discussed here.

SpiroZin4). These zinc binding units have been used to tune the affinity of fluorescein-based zinc sensors.[45]

In addition to these modifications, derivatives of SpiroZin1 and SpiroZin2 (Figure 4.2) were functionalized with a carboxylic acid to make the corresponding SpiroZin1-COOH and SpiroZin2-COOH. The purpose of introducing the carboxylic acid is to allow for conjugation of the probe to intracellular targeting vectors. Using amide coupling reactions, the sensors can be conjugated to the *N*-terminus of peptides[77,78,79] or small molecules with specific intracellular localization properties, such as the aminoethyltriphenylphosphonium (TPP) ion.[80,81,82,83] These probes will be useful to monitor the trafficking of mobile zinc between subcellular locales, which is essential to understand the implications of its release and accumulation.

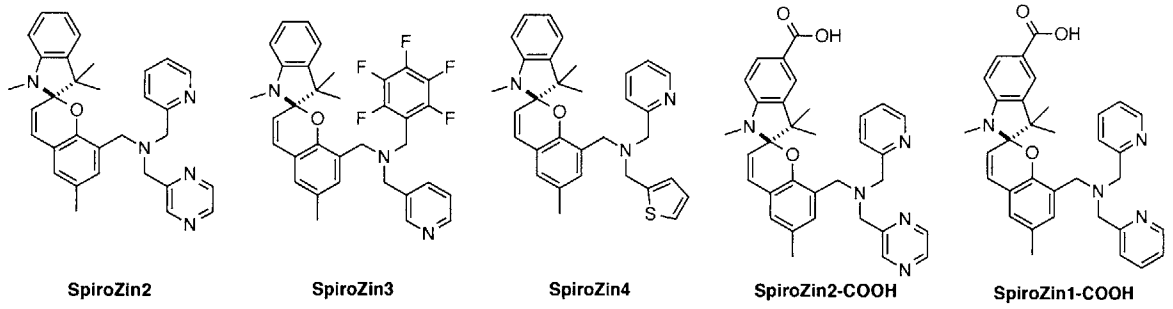

Figure 4.2. Structures of SpiroZin probes.

Several different methods can be used to target fluorophores and sensors in cells, including small molecules,[80] peptides,[77,78,79] and genetically encoded probes, such as the SNAP- and Halo-tag fusion proteins.[84,85,86] Using a combination of peptide-based and small-molecule strategies, attempts were made to target SpiroZin1-COOH and SpiroZin2-COOH to acidic vesicles, mitochondria, and the nucleus.

SpiroZin1 is pH-insensitive and therefore an ideal probe to monitor the levels of mobile zinc in acidic vesicles.[76] To target this probe to acidic vesicles, a peptide-based approach was used. The peptide constructed for this purpose was nonaarginine (R9), a cell-penetrating peptide.[87] Incubation of cells in medium containing low concentrations of R9 (~2 μM) leads to sequestration of the peptide in acidic vesicles.[88] To target SpiroZin2 to the mitochondria, the small molecule TPP was connected via amide bond formation to SpiroZin2-COOH. TPP is a lipophilic cation that has been used to target fluorescent sensors to mitochondria.[80,83]

Progress toward the preparation of a nuclear-targeted version of SpiroZin2 is reported in this chapter. This new probe, referred to as SpiroZin2-H, comprises a Hoechst dye functionalized with a primary amine that is connected via an amide linkage to SpiroZin2-COOH. The Hoechst dye binds to the minor groove of DNA at AT-rich regions. This dye was chosen because it is cell and nucleus permeable, displays bright blue fluorescence upon binding DNA, and its terminal phenol can be modified without losing its ability to bind DNA.[89,90,91]

4.2 Experimental Section

General Methods

All reactions were performed under a nitrogen atmosphere unless otherwise specified. Reagents and solvents were purchased or prepared as outlined in Chapter 2. NMR spectra were acquired on a Varian Mercury-300 instrument. ^{1}H NMR chemical shifts are reported in ppm relative to $SiMe_4$ ($\delta = 0$) and were referenced internally with respect to residual protons in the solvent ($\delta = 3.31$ for CD_3OD or $\delta = 2.50$ for DMSO-d_6). Low-

resolution mass spectra (LRMS) were acquired on an Agilent 1100 Series LC/MSD Trap spectrometer (LCMS), using electrospray ionization (ESI). Semipreparative HPLC separations were carried out on an Agilent 1200 HPLC instrument with a multiwavelength detector and automated fraction collector using a C18 reverse stationary phase (Zorbax-SB C18, 5 μm, 9.5 × 250 mm) and a mobile phase composed of two solvents (A: 0.1% (v/v) trifluoroacetic acid (TFA) in H_2O; B: 0.1% (v/v) TFA in CH_3CN). Specific purification protocols are described below for each compound. IUPAC names of all compounds are provided and were determined using CS ChemBioDrawUltra 12.0.

Synthesis and Coupling of SpiroZin1-COOH

*Synthesis of 2,2,6-Trimethyl-4H-benzo[d][1,3]dioxine-8-carbaldehyde (**1**).*

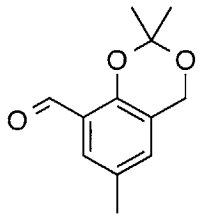

This compound was prepared according to a literature procedure.[92] Briefly, pyridinium chlorochromate (1.9 g, 8.6 mmol) was dissolved in dry CH_2Cl_2 (10 mL). (2,2,6-Trimethyl-4*H*-benzo[*d*][1,3]dioxin-8-yl)methanol (1.2 g, 5.8 mmol) was added in dry CH_2Cl_2 (10 mL) and the mixture was stirred for 1 h. The solvent was evaporated under reduced pressure and the solid was purified by column chromatography (SiO_2; CH_2Cl_2/CH_3OH 95:5) to give the product (0.98 g, yield 83%). ^1H NMR (300 MHz, $CDCl_3$): 1.59 (s, 6H), 2.28 (s, 3H), 4.85 (s, 2H), 7.01 (s, 1H), 7.52 (s, 1H), 10.38 (s, 1H).

*Synthesis of 3-(Chloromethyl)-2-hydroxy-5-methylbenzaldehyde (**2**).*

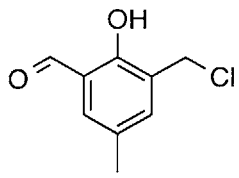

This compound was prepared according to a literature procedure.[92] Briefly, compound **1** (608 mg, 2.9 mmol) was suspended in concentrated HCl (13 mL) and stirred overnight. The suspension was transferred to a Falcon tube and centrifuged. The supernatant was decanted and the solid was washed with water (20 mL). The precipitate was redissolved in CH_2Cl_2, dried with Na_2SO_4, and the solvent was evaporated under reduced pressure to give the product as a light purple solid (446 mg, 82%). Mp: 60–70 °C. ^{1}H NMR (300 MHz, $CDCl_3$): 2.35 (s, 3H), 4.66 (s, 2H), 7.34 (d, ^4J = 3 Hz, 1H), 7.46 (d, ^4J = 3 Hz, 1H), 9.86 (s, 1H), 11.25 (s, 1H).

*Synthesis of 5-Carboxy-1,2,3,3-tetramethyl-3H-indol-1-ium Iodide (**3**).*

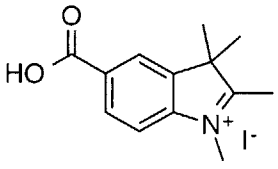

This compound was prepared according to a literature procedure.[93] Briefly, 2,3,3-trimethyl-3*H*-indole-5-carboxylic acid (617 mg, 3.0 mmol) was dissolved in a mixture of CH_3CN/toluene (1:2 v/v, 25 mL). CH_3I (188 μL, 3.0 mmol) was added and the mixture heated to reflux overnight. The reaction was cooled to room temperature and placed into an ice bath and the precipitate was collected, washed with EtOH and hexanes, and dried under vacuum to give the product as an orange solid (280 mg, yield 27%). LRMS (ESI). Calcd for $[C_{13}H_{16}NO_2]^+$: 218.3, found 218.1. ^{1}H NMR (300 MHz, DMSO-d_6): 1.54 (s, 6H), 2.78 (s, 3H), 3.97 (s, 3H), 8.00 (d, ^3J = 6 Hz, 1H), 8.18 (d, ^3J = 9 Hz, 1H), 8.36 (s, 1H).

Synthesis of (R)-8-((bis(Pyridine-2-ylmethyl)amino)methyl)-1',3',3',6-tetramethylspiro-[chromene-2,2'-indoline]-4'-carboxylic Acid (SpiroZin1-COOH).

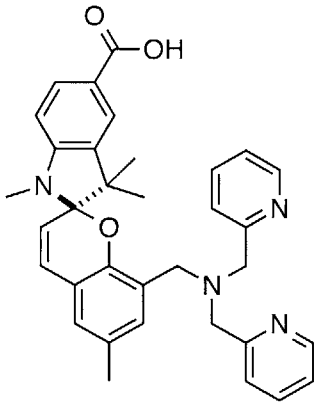

Compound **2** (100 mg, 0.54 mmol) and K_2CO_3 (224 mg, 1.63 mmol) were dissolved in CH_3CN (2.5 mL). DPA (195 μL, 1.1 mmol) was added in CH_3CN (2.5 mL) and the reaction was stirred at room temperature for 1 h. Compound **3** (186 mg, 0.54 mmol) was added in one portion and the reaction was heated to reflux for 1 h. The solvent was evaporated under reduced pressure and the solid was purified by column chromatography (SiO_2; CH_2Cl_2/CH_3OH 95:5, 2% CH_3COOH). The product was further purified by RP-HPLC according to the following protocol: constant flow rate 3 mL min^{-1}; isocratic flow 2% B, 0–5 min; gradient 2–35 % B, 5–10 min; gradient 35–75% B, 10–20 min; gradient 75–95% B, 20–28 min. The product was collected between 14–17.2 min. All equivalent fractions recovered from independent runs were combined and lyophilized to dryness to yield the TFA salt of SpiroZin1-COOH. (~50 mg). LRMS (ESI). Calcd for $[C_{34}H_{35}N_4O_3]^+$: 547.7, found 547.5. ^{1}H NMR (300 MHz, DMSO-d_6): 1.09 (s, 3H), 1.17 (s, 3H), 2.17 (s, 3H), 2.68 (overlapped d), 2.70 (overlapped s), 4.16 (overlapped d, ^3J = 9 Hz), 5.82 (d, ^3J = 12 Hz, 1H), 6.52 (d, ^3J = 9 Hz, 1H), 7.05 (m, 2H), 7.28 (d, ^3J = 9 Hz, 2H), 7.35 (m, 2H), 7.60 (d, ^3J = 3 Hz, 1H), 7.82 (d, ^3J = 3 Hz, 1H), 7.77 (d, ^3J = 3 Hz, 1H), 7.80 (d, ^3J = 3 Hz, 1H), 8.46 (d, ^3J = 9 Hz, 2H).

Synthesis of ((R)-8-((bis(Pyridin-2-ylmethyl)amino)methyl)-1',3',3',6-tetramethylspiro-[chromene-2,2'-indoline]-4'-carbonyl)alanine (SpiroZin1-Ala).

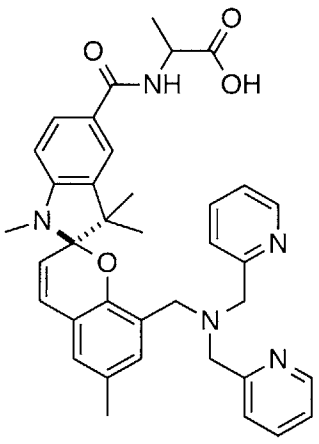

HATU (15 mg, 0.04 mmol) and SpiroZin1-COOH (21 mg, 0.04 mmol) were dissolved in dry DMF (1 mL). Diisopropylethylamine (0.1 mL) was added and the reaction mixture stirred for 10 min. L-Alanine (3.4 mg, 0.04 mmol) was added in one portion and the mixture was stirred for 5 h. The product was stored in DMF and used without further purification. LRMS (ESI). Calcd for $[C_{37}H_{40}N_5O_4]^+$: 618.8, found 618.3.

Synthesis of SpiroZin1-R9 and SpiroZin1-Ala-R9

The R9 peptide (NH_2-RRRRRRRRR-$CONH_2$) was prepared by solid-phase peptide synthesis using an Aapptec Focus Xi automated peptide synthesizer. FMOC groups were removed by treating the protected resin (100 mg, ~0.06 mmol) with a solution of 4-methylpiperidine (20% v/v in dry DMF) for 2 x 10 min periods. For coupling reactions, FMOC-Arg(Pbf)-OH (158 mg, 0.24 mmol) was combined as a solid with solid HATU (93 mg, 0.24 mmol). Immediately prior to the coupling reaction, the mixture was dissolved in a freshly prepared solution of DIPEA (10% v/v in dry DMF). The resin was allowed to react in the coupling solution for 30 min.

Attempts to couple SpiroZin1-COOH and SpiroZin1-Ala to the R9 peptide were performed manually in a fritted 2.5 mL syringe according to a modified literature protocol[94] and briefly described here. The resin-bound R9 peptide (~0.03 mmol) was

swelled for 1 h in dry DMF (2 mL). *N*-terminal FMOC groups were removed by shaking the resin with a solution of 4-methylpiperidine (1.5 mL, 20% v/v in dry DMF) for 10 min or 7 h, followed by a wash with dry DMF (5 x 1.5 mL). The coupling was either performed immediately or after drying the resin under vacuum overnight. For the coupling, SpiroZin1-COOH (0.12 mmol) or SpiroZin1-Ala (~0.03 mmol) were combined with HATU (1 equiv) and dissolved in DIPEA (1.5 mL, 10% v/v in dry DMF) and shaken for 10 min or overnight. After coupling, the resin was washed with dry DMF (5 x 1.5 mL), CH_2Cl_2 (5 x 1.5 mL), and dried under vacuum for 1 h or overnight. SpiroZin1-R9 or SpiroZin1-Ala-R9 was cleaved from the resin by treating with a TFA/water/triisopropylsilane solution (1.5 mL, 95/2.5/2.5% v/v) for 90 min or 4 h. The resulting crude peptide was purified by RP-HPLC according to the following protocol: constant flow rate 3 mL min^{-1} ; isocratic flow 5% B, 0–5 min; gradient 5–50% B, 5–35 min; gradient 50–95% B, 35–40 min; isocratic flow 95% B, 40–45 min. No product was isolated following HPLC purification.

Synthesis of SprioZin2, SpiroZin2-COOH, SpiroZin2-TPP, and SpiroZin2-H

*Synthesis of 1-(Pyrazin-2-yl)-N-(pyridin-2-ylmethyl)methanamine (**4**).*

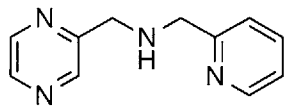

Pyrazine-2-carbaldehyde (100 mg, 0.93 mmol) and 2-aminomethyl-pyridine (95 μL, 0.93 mmol) were dissolved in CH_3OH and stirred overnight. $NaBH_4$ (105 mg, 2.8 mmol) was added in one portion. After 1 h, the solvent was evaporated under reduced pressure and the residue was redissolved in a mixture of CH_2Cl_2/H_2O and the phases were separated. The organic phase was dried with Na_2SO_4, filtered, and the solvent was evaporated under reduced

pressure to give the product as a pale yellow oil (150 mg, yield 81%). LRMS (ESI). Calcd for $[C_{11}H_{13}N_4]^+$: 201.2, found 201.1. ^{1}H NMR (300 MHz, $CDCl_3$): 3.98 (d, ^3J = 12 Hz, 4H), 7.14 (t, ^3J = 6 Hz, 1H), 7.30 (d, ^3J = 6 Hz, 1H), 7.62 (m, 1H), 8.42 (s, 1H), 8.49 (s, 1H), 8.53 (d, ^3J = 6 Hz, 1H), 8.62 (s, 1H).

Synthesis of (R)-1-(Pyrazin-2-yl)-N-(pyridin-2-ylmethyl)-N-((1',3',3',6-tetramethylspiro-[chromene-2,2'-indolin]-8-yl)methyl)methanamine (SpiroZin2).

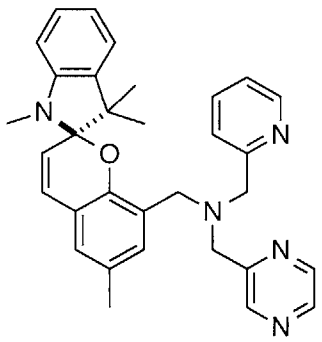

Compound **2** (50 mg, 0.27 mmol) and K_2CO_3 (113 mg, 0.82 mmol) were dissolved in CH_3CN (1.5 mL). Compound **4** (47 μL, 0.27 mmol) was added in CH_3CN (1.5 mL) and the mixture was stirred for 1 h. 1,2,3,3-Tetramethyl-3*H*-indol-1-ium iodide (see Chapter 2, compound **6**, 47 mg, 0.27 mmol) was added in one portion and the mixture heated to reflux for 1 h. The solvent was evaporated under reduced pressure and the residue purified by RP-HPLC according to the following protocol: constant flow rate 3 mL min^{-1}; isocratic flow 2% B, 0–5 min; gradient 2–35 % B, 5–10 min; gradient 35–75% B, 10–20 min; gradient 75–95% B, 20–28 min. The product was collected between 12.5–14.5 min. All equivalent fractions recovered from independent runs were combined and lyophilized to dryness to yield the TFA salt of SpiroZin2. (~15 mg) LRMS (ESI). Calcd for $[C_{32}H_{34}N_5O]^+$: 504.6, found 504.2. ^{1}H NMR (300 MHz, CD_3OD): 1.14 (s, 3H), 1.26 (s, 3H), 2.19 (s, 3H), 2.68 (s, 3H), 3.40 (d, ^2J = 12 Hz, 1H), 3.57 (d, ^2J = 12 Hz, 1H), 3.65 (m, 4H), 5.74 (d, ^3J = 12 Hz), 6.46 (d, ^3J = 9 Hz, 1H), 6.75 (dd, ^4J = 3 Hz, ^3J = 6 Hz, 1H), 6.80 (dd, ^4J = 3 Hz, ^3J = 6 Hz, 1H), 6.88 (d, ^3J = 9 Hz), 6.94 (d, ^3J = 3 Hz, 1 H), 7.02–7.08 (m,

2H), 7.20 (m, 1H), 7.38 (d, ^4J = 9 Hz, 2H), 7.65 (dt, ^4J = 3 Hz, ^3J = 9 Hz, 1H), 8.32–8.35 (m, 2H), 8.40 (m, 1H), 8.48 (d, ^4J = 3 Hz, 1H).

Synthesis of (R)-1',3',3',6-Tetramethyl-8-(((pyrazin-2-ylmethyl)(pyradin-2-ylmethyl)-amino)methyl)spiro[chromene-2,2'-indoline]-4'-carboxylic Acid (SpiroZin2-COOH).

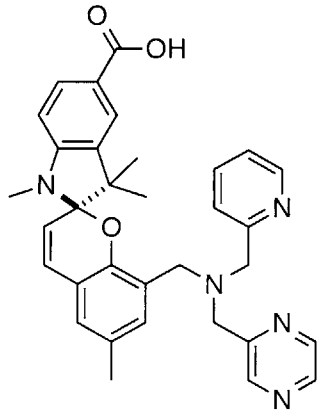

Compound **2** (61 mg, 0.35 mmol) and K_2CO_3 (145 mg, 1.05 mmol) were dissolved in CH_3CN (2 mL). Compound **4** was added in CH_3CN (2 mL) and the mixture was stirred for 1 h. Compound **3** (61 mg, 0.35 mmol) was added in one portion and the reaction was heated to reflux for 1 h. The solvent was evaporated under reduced pressure and the residue was purified by column chromatography (SiO_2; CH_2Cl_2/CH_3OH 9:1) to give the product as a colorless solid (60 mg, yield 44%) LRMS (ESI). Calcd for $[C_{33}H_{34}N_5O_3]^+$: 548.7, found 548.2. ^{1}H NMR (300 MHz, $CDCl_3$): 1.18 (s, 3H), 1.30 (s, 3H), 2.22 (s, 3H), 2.75 (s, 3H), 2.76 (d, ^2J = 9 Hz, 1H), 2.87 (d, ^2J = 9 Hz, 1H), 3.79 (bs, 4H), 5.66 (d, ^3J = 9 Hz, 1H), 6.48 (d, ^3J = 9 Hz, 1H), 6.79 (s, 1H), 6.80 (d, ^3J = 9 Hz, 1H), 7.18 (m, 2H), 7.45 (d, ^3J = 12 Hz, 1H), 7.60 (m, 1H), 7.78 (d, ^3J = 3 Hz, 1H), 7.98 (dd, ^4J = 3 Hz, ^3J = 9 Hz, 1H), 8.38 (m, 2H), 8.51 (d, ^3J = 3 Hz, 1H), 8.67 (s, 1H).

*Synthesis of (2-Aminoethyl)triphenylphosphonium Bromide (**5**)*

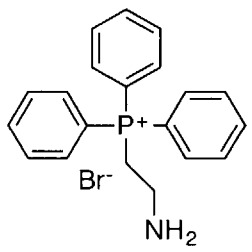

This compound was prepared according to a literature procedure.[95] Briefly, 2-bromoethan-1-amine (777 mg, 3.8 mmol) and triphenylphosphine (1.0 g, 3.8 mmol) were dissolved in CH_3CN.

The mixture was heated to reflux overnight. The precipitate was collected and redissolved in water. Solid Na_2CO_3 was added until the solution reached pH 11 and was extracted with CH_2Cl_2. The organic phase was dried with Na_2SO_4, filtered, and the solvent was evaporated under reduced pressure to give the product as a white solid (527 mg, yield 30%). Mp: 210–215 °C. LRMS (ESI). Calcd for $[C_{20}H_{21}NP]^+$: 306.4, found 306.2. ^{1}H NMR (300 MHz, $CDCl_3$): 3.22 (m, 2H), 4.18 (m, 2H), 7.64–7.89 (m, 15H).

Synthesis of (R)-Triphenyl(2-(1',3',3',6-tetramethyl-8-(((pyrazin-2-ylmethyl)-(pyridin-2-ylmethyl)amino)methyl)spiro[chromene-2,2'-indoline]-5'-carboxamido)ethyl)-phosphonium (SpiroZin2-TPP)

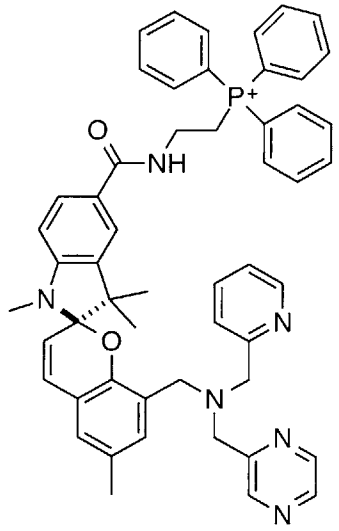

SpiroZin2-COOH (25 mg, 0.05 mmol) and HATU (17 mg, 0.05 mmol) were dissolved in dry DMF (1 mL). Diisopropylethylamine (100 μL) was added and the mixture was stirred for 10 min. Compound **5** (19 mg, 0.05 mmol) was added in one portion and the mixture was stirred overnight. The solvent was evaporated under reduced pressure and the solid was purified by column chromatography (SiO_2; CH_2Cl_2/CH_3OH 9:1). The product was further purified by RP-HPLC according to the following protocol: constant flow rate 3 mL min^{-1} ; isocratic flow 2% B, 0–5 min; gradient 2–35 % B, 5–10 min; gradient 35–75% B, 10–20 min; gradient 75–95% B, 20–28 min. The product was collected between 15.0–19.1 min. All equivalent fractions recovered from independent runs were combined and lyophilized to dryness to

yield the TFA salt of SpiroZin2-TPP (~2 mg). LRMS (ESI). Calcd for $[C_{54}H_{35}N_5O_2P]^+$: 835.02, found 835.7. ^{1}H NMR (300 MHz, $CDCl_3$): 1.15 (s, 3H), 1.31 (s, 3H), 2.23 (s, 3H), 2.70 (s, 3H), 2.87 (m, 2H), 3.44–3.82 (overlapped m, 8H), 5.62 (d, ^3J = 9 Hz), 6.43 (d, ^3J = 9 Hz), 6.77 (s, 1H), 6.80 (d, ^3J = 12 Hz), 7.09 (s, 1H), 7.59–7.80 (overlapped m, 20H), 8.36–8.40 (m, 2H), 8.60 (s, 1H).

*Synthesis of 2-(4-Cyanophenyl)-1H-benzo[d]imidazole-6-carboxylic Acid (**6**)*

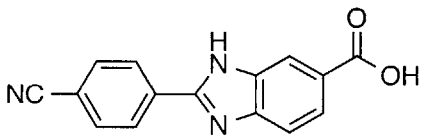

This compound was prepared according to a literature procedure.[96] Briefly, 4-formylbenzonitrile (500 mg, 3.8 mmol) and 3,4-diaminobenzoic acid (580 mg, 3.8 mmol) were dissolved in nitrobenzene (17 mL) and heated to reflux for 1 h. DMF (3 mL) was added to dissolve the precipitate. After 5 h, the reaction was cooled on ice and the precipitate was washed with hexanes to give the product as a light brown solid (443 mg, yield 44%). ^{1}H NMR (300 MHz, DMSO-d_6): 7.68 (s, 1H), 7.86 (d, ^3J = 9 Hz, 1H), 8.04 (d, ^3J = 9 Hz, 2H), 8.21 (s, 1H), 8.34 (d, ^3J = 9 Hz, 2H).

*Synthesis of 5-(4-Methylpiperazin-1-yl)-2-nitroaniline (**7**)*

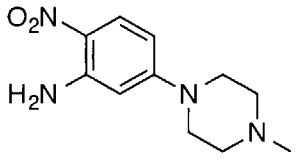

This compound was prepared according to a modified literature protocol.[96] 5-Chloro-2-nitroaniline (500 mg, 2.9 mmol) was dissolved in EtOH (3 mL). 1-Methylpiperazine (1350 μL, 12.2 mmol) was added and the reaction mixture was heated to reflux overnight. The mixture was cooled to room temperature and H_2O (4 mL) was added. The mixture was stirred for 1 h at room temperature and the precipitate was filtered, washed with H_2O and

isolated as a bright yellow solid (yield: 645 mg, 94%). ^{1}H NMR (300 MHz, DMSO-d_6): 2.18 (s, 3H), 2.38 (t, ^3J = 3 Hz, 4H), 3.29 (overlapped t), 6.19 (d, ^4J = 3 Hz, 1H), 6.38 (dd, ^4J = 3 Hz, ^3J = 12 Hz, 1H), 7.78 (d, ^3J = 12 Hz, 1H).

*Synthesis of 4-(4-Methylpiperazin-1-yl)benzene-1,2-diamine (**8**)*

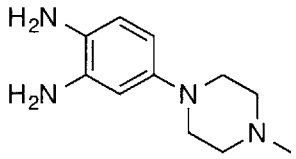

This compound was prepared according to a modified literature protocol.[97] Compound **7** (645 mg, 2.7 mmol) and Pd/C (64 mg) were dissolved in EtOH (5 mL) in a Parr bomb and stirred under H_2 (344 kPa). After 48 h, the suspension was filtered through Celite and the solvent was removed under reduced pressure to give the product as a light brown solid (233 mg, yield 40%). LRMS (ESI). Calcd for $[C_{11}H_{19}N_4]^+$: 207.3, found 207.2. ^{1}H NMR (300 MHz, DMSO-d_6): 2.17 (s, 3H), 2.39 (t, ^3J = 6 Hz, 4H), 2.84 (t, ^3J = 6 Hz, 4H), 5.99 (dd, ^4J = 3 Hz, ^3J = 9 Hz, 1H), 6.18 (d, ^4J = 3Hz, 1H), 6.36 (d, ^3J = 9 Hz, 1H).

*Synthesis of N-(2-Amino-4-(4-methylpiperazin-1-yl)phenyl)-2-(4-cyanophenyl)-1H-benzo[d]imidazole-6-carboxamide (**9**).*

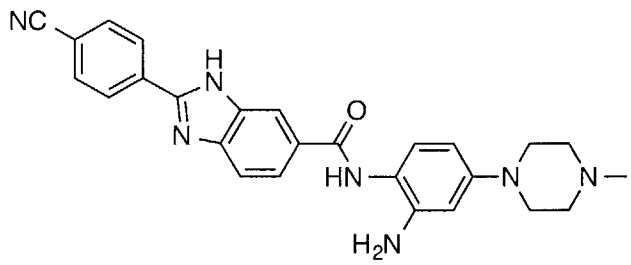

This compound was prepared according to a modified literature protocol.[96] Compound **6** (64 mg, 0.24 mmol) and HBTU (92 mg, 0.24 mmol) were dissolved in dry DMF (2.5 mL). Diisopropylethylamine (100 μL) was added and the mixture was stirred for 10 min. Compound **8** (50 mg, 0.24 mmol) was added in one portion. After 3 h, H_2O (10 mL) was added and the precipitate was

collected, washed with diethyl ether, and dried under vacuum to give the product as a light brown solid (66 mg, yield 60%). LRMS (ESI). Calcd for $[C_{26}H_{26}N_7O]^+$: 452.5, found 452.3. ^{1}H NMR (300 MHz, DMSO-d_6): 2.21 (s, 3H), 2.47 (overlapped t), 3.05 (t, ^3J = 9 Hz, 4H), 4.76 (s, 2H), 6.22 (d, ^3J = 3 Hz, 1H), 6.36 (d, ^3J = 3 Hz, 1H), 6.98 (d, ^3J = 9 Hz, 1H), 7.90 (s, 1H), 8.03 (s, 1H), 8.06 (s, 1H), 8.35 (m, 3H), 9.56 (d, ^3J = 9 Hz, 1H).

*Synthesis of 4-(6-(4-Methylpiperazin-1-yl)-1H,3'H-[2,5'-bibenzo[d]imidazol]-2'-yl)-benzonitrile (**10**).*

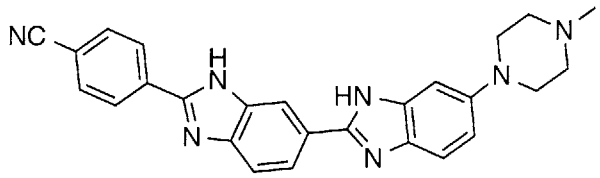

Compound **9** (66 mg, 0.15 mmol) was dissolved in CH_3COOH (12 mL) and heated to reflux overnight. The solvent was evaporated, and the solid was washed with diethyl ether to give the product as a light brown solid (63 mg, yield 98%). LRMS (ESI). Calcd for $[C_{26}H_{24}N_7]^+$: 434.5, found 434.5. ^{1}H NMR (300 MHz, DMSO-d_6): 2.24 (s, 3H), 2.50 (overlapped t), 3.12 (overlapped t), 6.93 (m, 2H), 7.45 (s, 1H), 7.76 (d, ^3J = 9 Hz, 1H), 8.04 (m, 3H), 8.37 (m, 3H).

*Synthesis of (4-(6-(4-Methylpiperazin-1-yl)-1H,3'H-[2,5'-bibenzo[d]imidazol]-2'-yl)-phenyl)methanamine (**11**).*

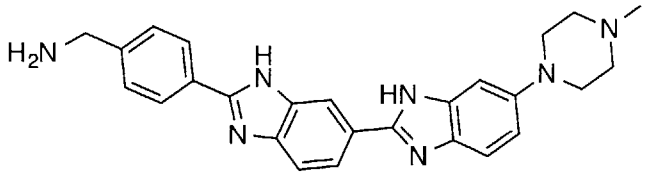

Compound **10** (63 mg, 0.14 mmol) was dissolved in a mixture of CH_3OH (5 mL) and HCl in CH_3OH (5 mL).

Pd/C (30 mg) was added and the mixture was stirred under an atmosphere of H_2. After 24 h, the mixture was filtered through Celite, which was washed with CH_3OH, and the solvent was evaporated under reduced pressure. The product used without further purification. LRMS (ESI). Calcd for $[C_{26}H_{28}N_7]^+$: 438.6, found 438.3.

Synthesis of (R)-1',3',3',6-Tetramethyl-N-(4-(6-(4-methylpiperazin-1-yl)-1H,3'H-[2,5'-bibenzo[d]imidazol]-2'-yl)benzyl)-8-(((pyrazin-2-ylmethyl)(pyridin-2-ylmethyl)amino)-methyl)spiro[chromene-2,2'-indoline]-5'-carboxamide (SpiroZin2-H).

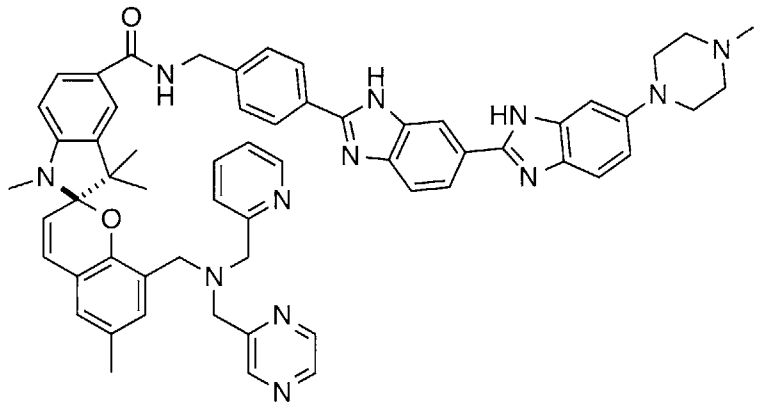

SpiroZin2-COOH (5 mg, 0.0085 mmol) and HBTU (3 mg, 0.0085 mmol) were dissolved in dry DMF (0.5 mL). DIPEA (100 μL) was added and the mixture was stirred for 10 min. Compound **11** (5 mg, 0.0085 mmol) was added in dry DMF (500 μL). The mixture was stirred for 3 h, poured onto ice, and the precipitate was collected. LRMS (ESI). Calcd for $[C_{59}H_{59}N_{12}O_2]^+$: 967.5, found 967.6.

Synthesis of SpiroZin4

*Synthesis of 1-(Pyridine-2-yl)-N-(thiophen-2-ylmethyl)methanamine (**12**).*

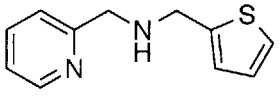

2-Formylthiophene (2.1 g, 18.5 mmol) was added to a Schlenk flask. 2-Aminomethyl-pyridine (2.0 g, 18.5 mmol) dissolved in CH_3OH (20 mL) was added dropwise and the solution was stirred overnight at room

temperature. $NaBH_4$ (2.1 g, 37.8 mmol) was added and the mixture was heated to reflux for 3 h. The solvent was evaporated and the crude oil was dissolved in a mixture of CH_2Cl_2 and H_2O and extracted with CH_2Cl_2, dried with Na_2SO_4, and filtered. The solvent was evaporated under reduced pressure to give the product as a pale yellow oil (2.6 g, 70%). LCMS (ESI). Calcd for $[C_{10}H_{11}N_3S]^+$: 205.3, found 205.1. ^{1}H NMR (300 MHz, DMSO-d_6): 3.80 (s, 2H), 3.89 (s, 2H), 6.94 (m, 2H), 7.21 (t, ^3J = 6 Hz, 1H), 7.36 (t, ^3J = 3 Hz, 1H), 7.42 (d, ^3J = 9 Hz, 1H), 7.72 (m, 1H), 8.48 (d, ^3J = 3 Hz, 1H).

Synthesis of (R)-1-(Pyridin-2-yl)-N-((1',3',3',6-tetramethylspiro[chromene-2,2'-indolin]-8-yl)methyl)-N-(thiophen-2-ylmethyl)methanamine (SpiroZin4).

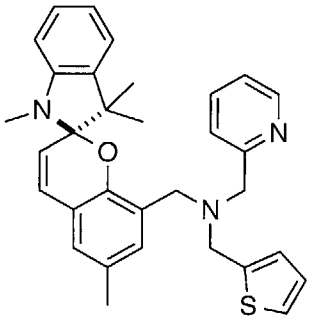

Compound **2** (50 mg, 0.27 mmol) and K_2CO_3 (112 mg, 0.81 mmol) were dissolved in CH_3CN (1.5 mL). Compound **12** (55 mg, 0.27 mmol) was added in CH_3CN (1.5 mL) and stirred at room temperature for 1 h. 1,2,3,3-Tetramethyl-3*H*-indol-1-ium iodide (see Chapter 2, compound **6**, 112 mg, 0.27 mmol) was added in one portion and the mixture was heated to reflux for 1 h. The solvent was evaporated under reduced pressure and purified by column chromatography (Al_2O_3; CH_2Cl_2/Hexanes 75:15). The product was further purified by RP-HPLC according to the following protocol: constant flow rate 3 mL min^{-1} ; isocratic flow 2% B, 0–5 min; gradient 2–35 % B, 5–10 min; gradient 35–75% B, 10–20 min; gradient 75–95% B, 20–28 min. The product was collected between 17–20 min. All equivalent fractions recovered from independent runs were combined and lyophilized to dryness to yield the TFA salt of SpiroZin4 (~20 mg). LRMS (ESI). Calcd for $[C_{32}H_{34}N_3OS]^+$: 508.7, found

508.2. ^{1}H NMR (300 MHz, DMSO-d_6): 1.07 (s, 3H), 1.17 (s, 3H), 2.18 (s, 3H), 2.57 (s, 3H), 3.26 (overlapped m, 1H), 3.50 (d, ^{2}J = 3 Hz, 1H), 3.58 (d, ^{2}J = 3 Hz, 1H), 5.71 (d, ^{3}J = 9 Hz, 1H), 6.50 (d, ^{3}J = 9 Hz, 1H), 6.75 (t, ^{3}J = 6 Hz, 1H), 6.84–6.95 (m, 4H), 7.07 (m, 3H), 7.18 (t, ^{3}J = 6 Hz, 1H), 7.35 (m, 2H), 7.67 (td, ^{3}J = 9 Hz, ^{4}J = 2 Hz, 1H), 8.40 (d, ^{3}J = 6 Hz, 1H).

Spectroscopic Methods

Spectroscopy techniques were similar to those outlined in Chapter 2. Stock solutions of SpiroZin2, SpiroZin2-TPP, and SpiroZin4 in DMSO were prepared in the 1–2 mM range and stored at –20 °C in 1 mL aliquots and thawed immediately before each experiment. All spectroscopic measurements were conducted in aqueous buffer containing 50 mM PIPES (pH 7.0) and 100 mM KCl.

Mammalian Cell Culture, Staining, and Imaging Procedures

HeLa cells were cultured as described in Chapter 3. Prior to imaging with SpiroZin2-TPP, the growth medium was replaced with dye-free DMEM containing 5 μM SpiroZin2-TPP, 3 μM Hoechst 33528 dye, 1 μM MitoTracker Green, and the cells were incubated for 30 min. Cells were rinsed with PBS buffer (2 x 2 mL), followed by addition of fresh dye-free DMEM and mounted on the microscope.

4.3 Results and Discussion

Synthesis and Coupling of SpiroZin1-COOH

The synthesis of SpiroZin1 is a one-pot procedure[76] that can be easily modified to make derivatives with alternative zinc binding sites or with an added carboxylic acid functional group. Two of the building blocks used in the preparation of the SpiroZin sensors are readily synthesized and will be described first. The primary alcohol of (2,2,6-trimethyl-4*H*-benzo[*d*][1,3]dioxin-8-yl)methanol was oxidized to the corresponding aldehyde using PCC to give compound **1**, which was subsequently deprotected and chlorinated to give compound **2** in a single step (Scheme 4.1).[92]

Scheme 4.1. Synthesis of Compound **2**. Reagents and conditions: (a) PCC, dry CH_2Cl_2, RT, 1 h, 83%, (b) conc. HCl, RT, 12 h, 82%. PCC = Pyridinium chlorochromate.

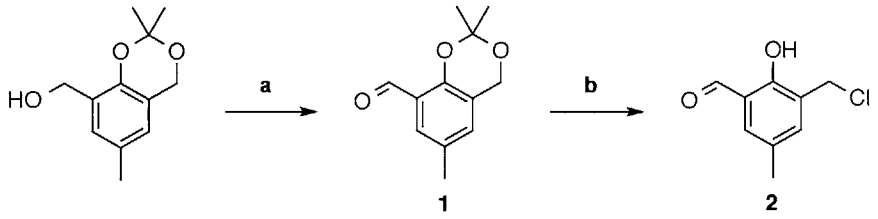

The second building block in the synthesis of the SpiroZin sensors with an added carboxylic acid was prepared by methylation of [2,3,3-trimethyl-3*H*-indole-5-carboxylic acid using methyl iodide to give compound **3** (Scheme 4.2).[93]

Scheme 4.2. Synthesis of Compound **3**. Reagents and conditions: (a) CH_3I, CH_3CN/Toluene, reflux, 12 h, 27%.

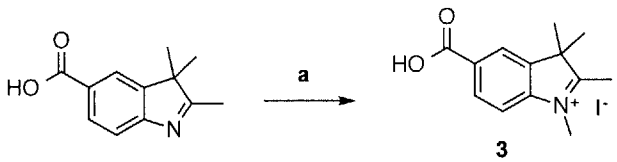

Using compounds **2**, **3**, and DPA, SpiroZin1-COOH was synthesized according to the procedure used for SpiroZin1.[76] DPA reacts with the benzylic chloride of compound **2**

in a nucleophilic substitution reaction. The intermediate formed undergoes Knoevenagel condensation with compound **3** to give SpiroZin1-COOH (Scheme 4.3). L-Alanine and SpiroZin1-COOH were coupled using HATU to form SpiroZin1-Ala (Scheme 4.3).

Scheme 4.3. Synthesis of SpiroZin1-COOH and SpiroZin1-Ala. Reagents and conditions: (a) DPA, K_2CO_3, CH_3CN, RT to reflux, 2 h, ~17%, (b) HATU, DIPEA, DMF, RT, 5 h. DPA = dipicolylamine, DIPEA = diisopropylethylamine.

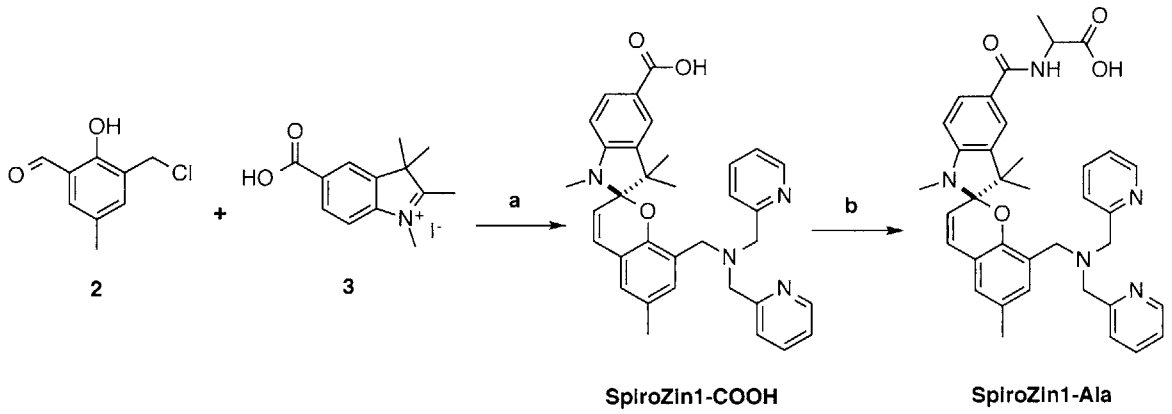

Attempts to couple SpiroZin1-COOH and SpiroZin1-Ala to the R9 peptide have been unsuccessful. Several problems were encountered while trying to optimize the reaction conditions for this coupling and will be discussed briefly. SpiroZin1-COOH was purified using RP-HPLC and isolated as the TFA salt. We noticed that the trifluoroacetate (TFA) counterion can react with HATU and subsequently couple to the *N*-terminus of the R9 peptide, interfering with its reaction with the sensor. The purification of sensors functionalized with carboxylates will be carried out in the absence of TFA to prevent these undesired reactions. Additionally, it was observed that the excess 4-methyl piperidine, which is used to cleave the FMOC protecting groups, can react with the HATU adduct of SpiroZin1-COOH, which inhibits its reaction with the R9 peptide as well. Longer drying time of the resin prior to FMOC deprotection failed to improve

results. Increasing the time for the coupling step, the deprotection, or the peptide cleavage from the resin also failed to yield the peptide-conjugated sensor. The conditions for this coupling reaction need to be further optimized and this project is ongoing.

Synthesis of SprioZin2, SpiroZin2-COOH, SpiroZin2-TPP, and SpiroZin2-H

The structure of SpiroZin1 was modified by changing the zinc binding site from a dipicolylamine to a methyl(pyrazine)picolylamine to make a second generation probe, SpiroZin2. The amine building block used in the preparation of this sensor, compound **4**, was synthesized by reductive amination of commercially available pyrazine-2-carbaldehyde with 2-(aminomethyl)pyridine (Scheme 4.4).

Scheme 4.4. Synthesis of Compound **4**. Reagents and conditions: (a) $NaBH_4$, CH_3OH, RT, 12 h, 81%.

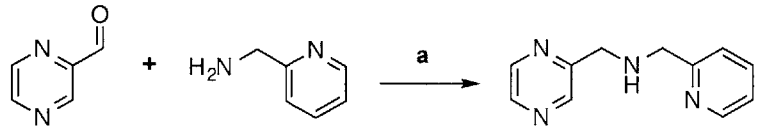

4

The syntheses of SpiroZin2 and SpiroZin2-COOH are analogous to those of SpiroZin1[76] and SpiroZin1-COOH (Schemes 4.5 and 4.6).

Scheme 4.5. Synthesis of SpiroZin2. Reagents and conditions: (a) K_2CO_3, CH_3CN, RT to reflux, 2 h.

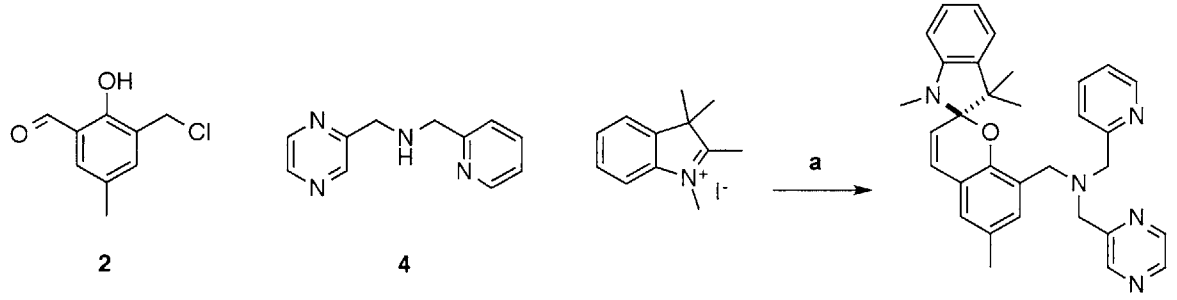

2 **4** **SpiroZin2**

Scheme 4.6. Synthesis of SpiroZin2-COOH. Reagents and conditions: (a) K_2CO_3, CH_3CN, RT to reflux, 2 h, 44%.

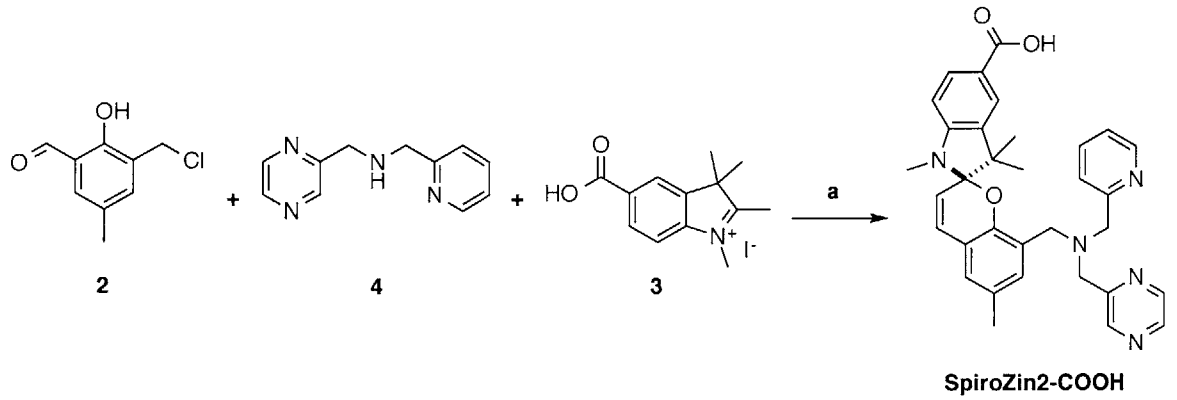

One method used to target fluorescent sensors to mitochondria is via conjugation to TPP.[80] The TPP ion was prepared by reaction of triphenylphosphine with 2-bromoethan-1-amine[95] to give compound **5** (Scheme 4.7). Compound **5** was coupled to SpiroZin2-COOH using HATU as the activating agent to produce SpiroZin2-TPP (Scheme 4.7).

Scheme 4.7. Synthesis of SpiroZin2-TPP. Reagents and conditions: (a) 2-bromoethan-1-amine, CH_3CN, reflux, 12 h, 30%, (b) SpiroZin2-COOH, HATU, DIPEA, DMF, RT, 12 h, ~5%. DIPEA = diisopropylethylamine. Counterions are omitted for clarity.

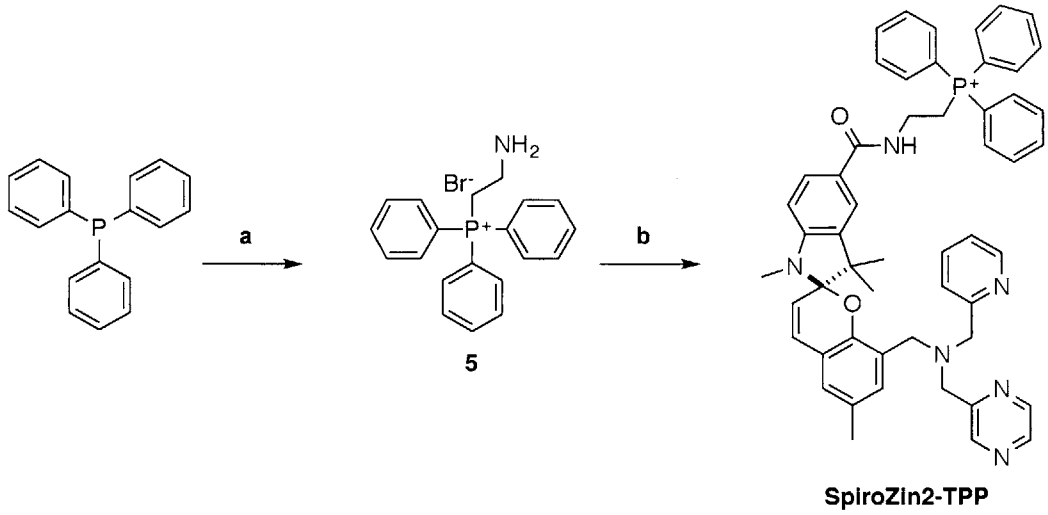

A targeting approach based on a small molecule was also attempted to direct SpiroZin2 to the nucleus of the cell. The small molecule selected for this targeting was the Hoechst dye functionalized with a primary amine. The synthesis of this dye started with the reaction of 4-cyanobenzaldehyde with 3,4-diaminobenzoic acid to give compound **6**.[96]

Scheme 4.8. Synthesis of Compound **6**. Reagents and conditions: (a) Nitrobenzene, DMF, reflux, 6 h, 44%.

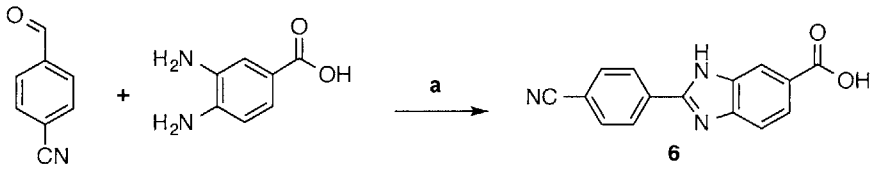

The attachment of the second benzimidazole ring took four additional steps and began with a nucleophilic aromatic substitution reaction between 5-chloro-2-nitroaniline and 1-methylpiperazine to give compound **7**, which was subsequently reduced to produce compound **8** (Scheme 4.9).[97]

Scheme 4.9. Synthesis of Compound **8**. Reagents and conditions: (a) EtOH, reflux, 12 h, 94%, (b) Pd/C, H_2, EtOH, RT, 48 h, 40%.

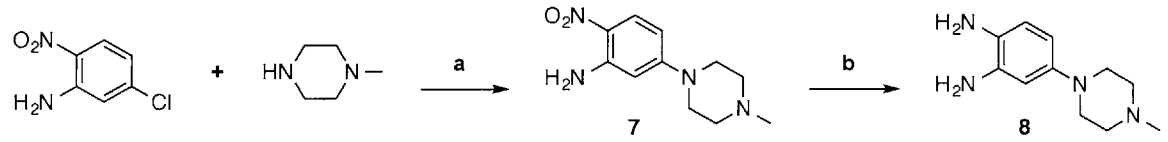

Compounds **6** and **8** were coupled using HBTU as the activating agent to generate compound **9** (Scheme 4.10). Compound **9** was used immediately in an acid-catalyzed ring closing reaction to give compound **10** (Scheme 4.10).

Scheme 4.10. Synthesis of Compound **10**. Reagents and conditions: (a) HBTU, DIPEA, DMF, RT, 3 h, 60%, (b) CH_3COOH, reflux, 12 h, 98%. DIPEA = diisopropylethylamine.

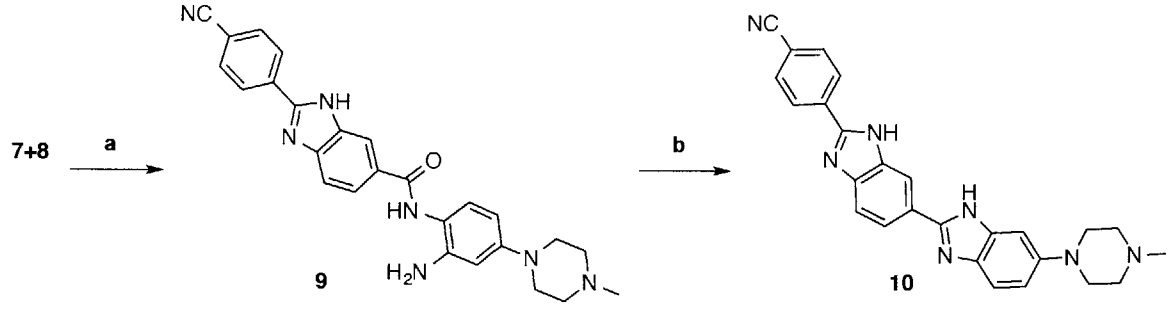

To produce the Hoechst dye functionalized with a primary amine, compound **10** was hydrogenated to yield compound **11** (Scheme 4.11), which was coupled to SpiroZin2-COOH to give SpiroZin2-H (Scheme 4.11).

Scheme 4.11. Synthesis of Compound **11**. Reagents and conditions: (a) Pd/C, H_2, CH_3OH, HCl/ CH_3OH, RT, 24 h (b) HBTU, DIPEA, DMF, 3 h. DIPEA = diisopropylethylamine.

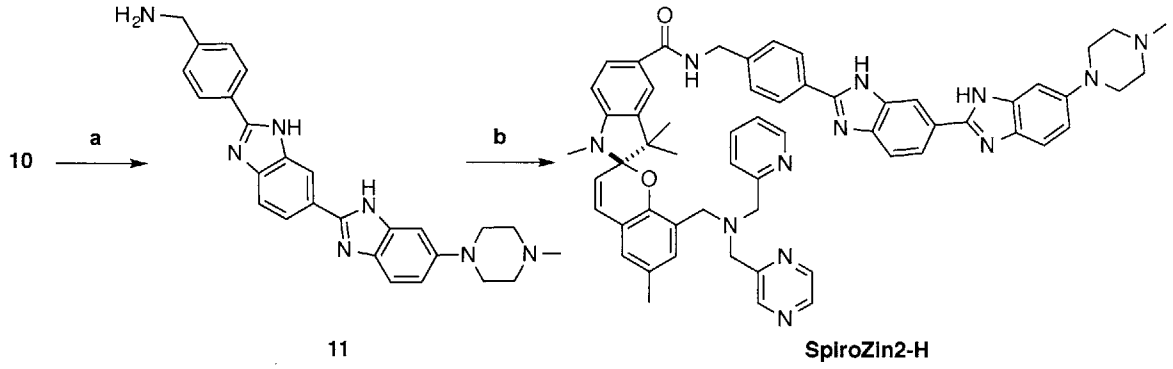

Synthesis of SpiroZin4

Sensor SpiroZin4 has a methyl(thiophene)picolylamine zinc binding unit. The amine building block used for the synthesis, compound **12**, was obtained from a reductive amination of 2-formylthiopene with 2-aminomethylpyridine (Scheme 4.12).

Scheme 4.12. Synthesis of Compound **12**. Reagents and conditions: (a) $NaBH_4$, CH_3OH, RT to reflux, 12 h, 70%.

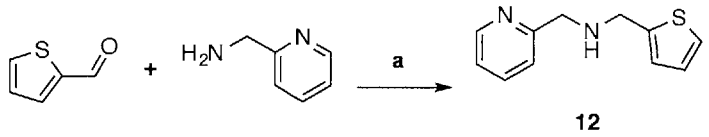

12

SpiroZin4 was synthesized in a one-pot procedure analogous to the synthesis of SpiroZin1 (Scheme 4.13).[76]

Scheme 4.13. Synthesis of SpiroZin4. Reagents and conditions (a) K_2CO_3, CH_3CN, RT to reflux, 2 h.

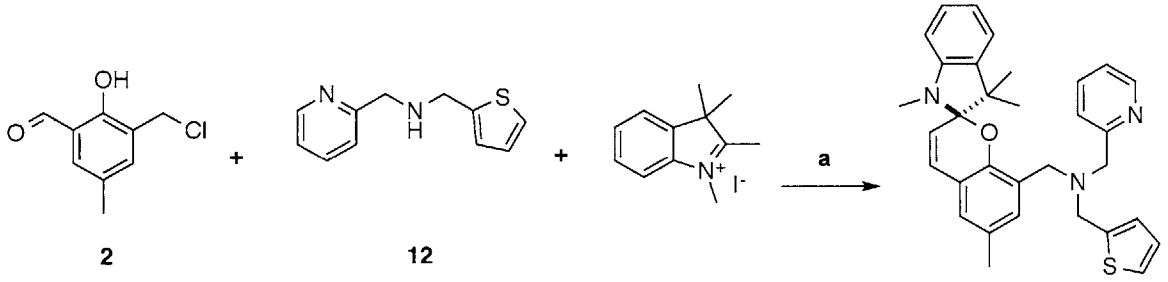

2 **12** **SpiroZin4**

Characterization of SpiroZin Sensors

The photophysical properties of SpiroZin2, SpiroZin2-TPP, and SpiroZin4 before and after addition of excess zinc were measured in aqueous buffer (50 mM PIPES, 100 mM KCl, pH 7) and are summarized in Figures 4.3 and 4.4. SpiroZin2 and SpiroZin2-TPP both exhibited similar photophysical properties. Upon excitation at 518 nm, both probes displayed a maximum in fluorescence intensity at 650 nm upon reaction with excess zinc, which is also similar to emission maximum of SpiroZin1.[76] The zinc-induced fluorescence response of SpiroZin2 and SpiroZin2-TPP in cuvettes is approximately 8- and 6-fold, respectively.

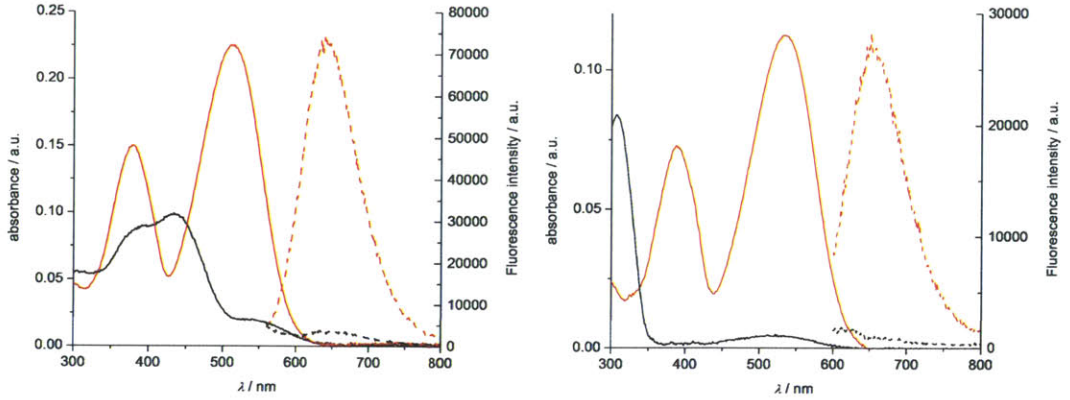

Figure 4.3. Photophysical properties of SpiroZin2 and SpiroZin2-TPP. (left) Fluorescence (dotted lines) and absorbance (solid lines) spectra of SpiroZin2 (left, black lines) and after addition of excess zinc (left, red lines) and SpiroZin2-TPP (right, black lines) and after reaction with excess zinc (right, red lines). in aqueous buffer (50 mM PIPES, 100 mM KCl, pH 7), λ_{ex} = 518 nm.

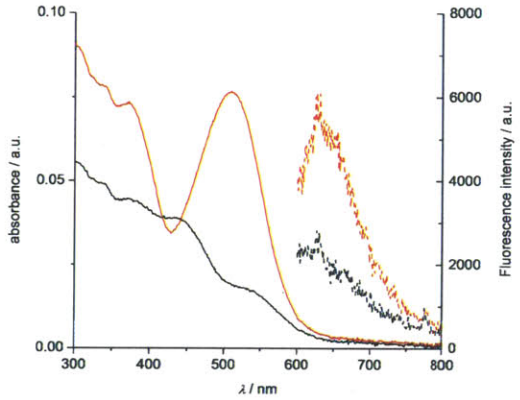

Figure 4.4. Photophysical properties of SpiroZin4. Fluorescence (dotted lines) and absorbance (solid lines) spectra of SpiroZin4 (black lines) and after addition of excess zinc (red lines) in aqueous buffer (50 mM PIPES, 100 mM KCl, pH 7), λ_{ex} = 518 nm.

SpiroZin4 does not detect zinc in cuvettes effectively (Figure 4.4). Given both its low absorbance and fluorescence enhancement upon reaction with excess zinc, SpiroZin4 was not further characterized or used. The reason for its low fluorescence turn-on has not been further investigated. SpiroZin2-H has not yet been characterized.

Live Cell Imaging

The ability of SpiroZin2-TPP to target mitochondria was investigated using HeLa cells incubated with 5 μM SpiroZin2-TPP and 1 μM MitoTracker Green. Upon addition of 30 μM of the cell permeable Zinc-pyrithione (ZnPT) complex, SpiroZin2-TPP displays

an approximate 40-fold fluorescence enhancement in live HeLa cells (Figure 4.5). The Pearson's correlation coefficient between SpiroZin2-TPP in the "on" fluorescence state and MitoTracker Green is 0.0032 ± 0.044, indicating no co-localization. The overlay of the two fluorescence channels is shown in Figure 4.6. Upon addition of TPEN, there is an approximate 10-fold decrease in fluorescence intensity in the red channel (Figure 4.5).

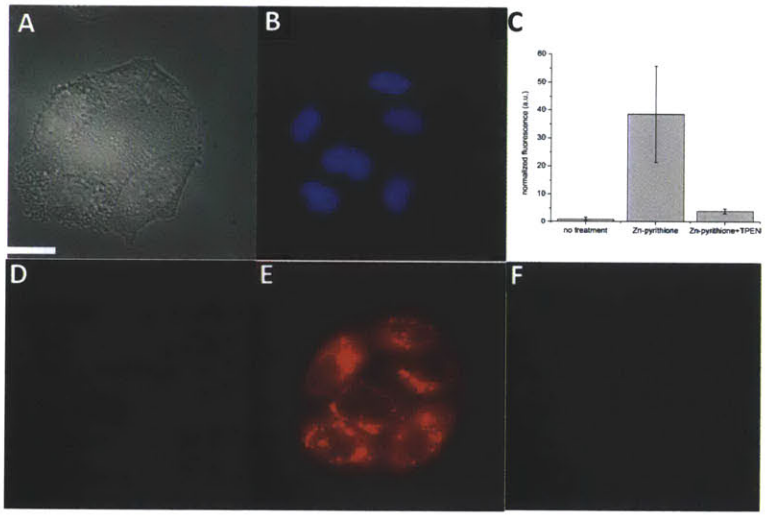

Figure 4.5. Turn-on response of SpiroZin2-TPP in HeLa cells. Fluorescence microscopy images of live HeLa cells incubated with 5 μM SpiroZin2-TPP in dye-free DMEM before and after addition of ZnPT and TPEN: (A) Differential interference contrast (DIC) image; (B) Blue channel showing nuclei; (C) Quantification; (D) Red channel before treatment; (E) Red channel after incubation for 10 min with 30 μM ZnPT; (F) Red channel after incubation for 10 min with 50 μM TPEN. Scale bar = 10 μm.

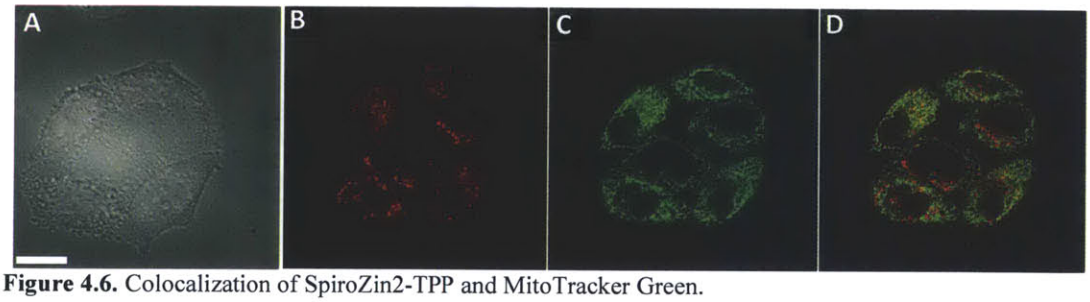

Figure 4.6. Colocalization of SpiroZin2-TPP and MitoTracker Green.
Fluorescence microscopy images of live HeLa cells incubated with 5 μM SpiroZin2-TPP in dye-free DMEM: (A) DIC image; (B) Deconvoluted red channel after incubation for 10 min with 30 μM ZnPT; (C) Deconvoluted green channel showing MitoTracker Green; (D) Overlay of deconvoluted red and green channels. Scale bar = 10 μm.

4.4 Conclusions

The work presented in this chapter is ongoing. The reaction conditions for the coupling of SpiroZin1-COOH to the R9 peptide need to be further optimized. The co-localization of SpiroZin2-TPP and MitoTracker Green has only been investigated using HeLa cells incubated with 5 μM SpiroZin2-TPP for 30 minutes. Future experiments need to be performed in which the concentration or incubation time of SpiroZin2-TPP is altered. Lower concentrations or longer incubation times may favor accumulation of SpiroZin2-TPP in the mitochondria. Finally, the synthesis of SpiroZin2-H needs to be repeated so that it may be purified, isolated, and used in cells to determine whether the Hoechst-dye functionalization directs the sensor to the nucleus.

References

(1) Lippard, S. J.; Berg, J. M. *Principles of Bioinorganic Chemistry 1st Ed.*; University Science Books: Mill Valley, CA, 1994.

(2) Bogdan, C. *Nat. Immunol.* **2001**, *2*, 907-916.

(3) Palmer, R. M. J.; Ferrige, A. G.; Moncada, S. *Nature* **1987**, *327*, 524-526.

(4) Bredt, D. S.; Hwang, P. M.; Snyder, S. H. *Nature* **1990**, *347*, 768-770.

(5) Bult, H.; Boeckxstaens, G. E.; Pelckmans, P. A.; Jordaens, F. H.; Vanmaercke, Y. M.; Herman, A. G. *Nature* **1990**, *345*, 346-347.

(6) Kemp-Harper, B. K. *Antioxid. Redox Signal.* **2011**, *14*, 1609-1613.

(7) Bullen, M. L.; Miller, A. A.; Andrews, K. L.; Irvine, J. C.; Ritchie, R. H.; Sobey, C. G.; Kemp-Harper, B. K. *Antioxid. Redox Signal.* **2011**, *14*, 1675-1686.

(8) Paolocci, N.; Saavedra, W. F.; Miranda, K. M.; Martignani, C.; Isoda, T.; Hare, J. M.; Espey, M. G.; Fukuto, J. M.; Feelisch, M.; Wink, D. A.; Kass, D. A. *Proc. Natl. Acad. Sci. U.S.A.* **2001**, *98*, 10463-10468.

(9) Dautov, R. F.; Ngo, D. T. M.; Licari, G.; Liu, S.; Sverdlov, A. L.; Ritchie, R. H.; Kemp-Harper, B. K.; Horowitz, J. D.; Chirkov, Y. Y. *Nitric Oxide-Biol. Chem.* **2013**, *35*, 72-78.

(10) Choe, C. U.; Lewerenz, J.; Fischer, G.; Uliasz, T. F.; Espey, M. G.; Hummel, F. C.; King, S. B.; Schwedhelm, E.; Boger, R. H.; Gerloff, C.; Hewett, S. J.; Magnus, T.; Donzelli, S. *J. Neurochem.* **2009**, *110*, 1766-1773.

(11) Choe, C. U.; Lewerenz, J.; Gerloff, C.; Magnus, T.; Donzelli, S. *Antioxid. Redox Signal.* **2011**, *14*, 1699-1711.

(12) Zhang, Y. *J. Inorg. Biochem.* **2013**, *118*, 191-200.

(13) Flores-Santana, W.; Salmon, D. J.; Donzelli, S.; Switzer, C. H.; Basudhar, D.; Ridnour, L.; Cheng, R.; Glynn, S. A.; Paolocci, N.; Fukuto, J. M.; Miranda, K. M.; Wink, D. A. *Antioxid. Redox Signal.* **2011**, *14*, 1659-1674.

(14) Fukuto, J. M.; Carrington, S. J. *Antioxid. Redox Signal.* **2011**, *14*, 1649-1657.

(15) Mateo, A. O.; De Artinano, M. A. A. *Pharmacol. Res.* **2000**, *42*, 421-427.

(16) Eich, R. F.; Li, T. S.; Lemon, D. D.; Doherty, D. H.; Curry, S. R.; Aitken, J. F.; Mathews, A. J.; Johnson, K. A.; Smith, R. D.; Phillips, G. N.; Olson, J. S. *Biochemistry* **1996**, *35*, 6976-6983.

(17) Beckman, J. S.; Koppenol, W. H. *Am. J. Physiol.-Cell Physiol.* **1996**, *271*, C1424-C1437.

(18) Sakai, N.; Kaufman, S.; Milstien, S. *Mol. Pharmacol.* **1993**, *43*, 6-10.

(19) Adak, S.; Wang, Q.; Stuehr, D. J. *J. Biol. Chem.* **2000**, *275*, 33554-33561.

(20) Donzelli, S.; Espey, M. G.; Flores-Santana, W.; Switzer, C. H.; Yeh, G. C.; Huang, J. M.; Stuehr, D. J.; King, S. B.; Miranda, K. M.; Wink, D. A. *Free Radic. Biol. Med.* **2008**, *45*, 578-584.

(21) Murphy, M. E.; Sies, H. *Proc. Natl. Acad. Sci. U.S.A.* **1991**, *88*, 10860-10864.

(22) Sharpe, M. A.; Cooper, C. E. *Biochem. J.* **1998**, *332*, 9-19.

(23) Filipovic, M. R.; Miljkovic, J. L.; Nauser, T.; Royzen, M.; Klos, K.; Shubina, T.; Koppenol, W. H.; Lippard, S. J.; Ivanovic-Burmazovic, I. *J. Am. Chem. Soc.* **2012**, *134*, 12016-12027.

(24) Miljkovic, J. L.; Kenkel, I.; Ivanovic-Burmazovic, I.; Filipovic, M. R. *Angew. Chem. Int. Ed.* **2013**, *52*, 12061-12064.

(25) Vallee, B. L.; Falchuk, K. H. *Physiol. Rev.* **1993**, *73*, 79-118.

(26) Maret, W. In *Metallomics and the Cell*; Banci, L., Ed.; Springer: Dordrecht, 2013; Vol. 12, p 479-501.

(27) Frederickson, C. J.; Koh, J. Y.; Bush, A. I. *Nat. Rev. Neurosci.* **2005**, *6*, 449-462.

(28) Taylor, C. G. *Biometals* **2005**, *18*, 305-312.

(29) Franklin, R. B.; Milon, B.; Feng, P.; Costello, L. C. *Front. Biosci.* **2005**, *10*, 2230-2239.

(30) Kojda, G.; Harrison, D. *Cardiovasc. Res.* **1999**, *43*, 562-571.

(31) Heales, S. J. R.; Bolanos, J. P.; Stewart, V. C.; Brookes, P. S.; Land, J. M.; Clark, J. B. *Biochim. Biophys. Acta-Bioenerg.* **1999**, *1410*, 215-228.

(32) Hussain, S. P.; Hofseth, L. J.; Harris, C. C. *Nat. Rev. Cancer* **2003**, *3*, 276-285.

(33) Liu, Z. P.; He, W. J.; Guo, Z. J. *Chem. Soc. Rev.* **2013**, *42*, 1568-1600.

(34) Pluth, M. D.; Tomat, E.; Lippard, S. J. *Annu. Rev. Biochem.* **2011**, *80*, 333-355.

(35) Armstrong, D. A. H., R. E.; Lymar, S.; Koppenol, W. H.; Mereńyi, G.; Neta, P.; Stanbury, D.M.; Steenken, S.; Wardman, P.; *BioInorg. React. Mech.* **2014**, *9*, 59-61.

(36) Lee, K. Y.; Kuchynka, D. J.; Kochi, J. K. *Inorg. Chem.* **1990**, *29*, 4196-4204.

(37) Lim, M. H.; Wong, B. A.; Pitcock, W. H.; Mokshagundam, D.; Baik, M. H.; Lippard, S. J. *J. Am. Chem. Soc.* **2006**, *128*, 14364-14373.

(38) McQuade, L. E.; Pluth, M. D.; Lippard, S. J. *Inorg. Chem.* **2010**, *49*, 8025-8033.

(39) Rosenthal, J.; Lippard, S. J. *J. Am. Chem. Soc.* **2010**, *132*, 5536-5537.

(40) Royzen, M.; Wilson, J. J.; Lippard, S. J. *J. Inorg. Biochem.* **2013**, *118*, 162-170.

(41) Tennyson, A. G.; Do, L.; Smith, R. C.; Lippard, S. J. *Polyhedron* **2007**, *26*, 4625-4630.

(42) Zhou, Y.; Liu, K.; Li, J. Y.; Fang, Y. A.; Zhao, T. C.; Yao, C. *Org. Lett.* **2011**, *13*, 1290-1293.

(43) Apfel, U. P.; Buccella, D.; Wilson, J. J.; Lippard, S. J. *Inorg. Chem.* **2013**, *52*, 3285-3294.

(44) Kawai, K.; Ieda, N.; Aizawa, K.; Suzuki, T.; Miyata, N.; Nakagawa, H. *J. Am. Chem. Soc.* **2013**, *135*, 12690-12696.

(45) Nolan, E. M.; Lippard, S. J. *Acc. Chem. Res.* **2009**, *42*, 193-203.

(46) Hilderbrand, S. A.; Weissleder, R. *Curr. Opin. Chem. Biol.* **2010**, *14*, 71-79.

(47) Egawa, T.; Hirabayashi, K.; Koide, Y.; Kobayashi, C.; Takahashi, N.; Mineno, T.; Terai, T.; Ueno, T.; Komatsu, T.; Ikegaya, Y.; Matsuki, N.; Nagano, T.; Hanaoka, K. *Angew. Chem. Int. Ed.* **2013**, *52*, 3874-3877.

(48) Kobayashi, H.; Koyama, Y.; Barrett, T.; Hama, Y.; Regino, C. A. S.; Shin, I. S.; Jang, B. S.; Le, N.; Paik, C. H.; Choyke, P. L.; Urano, Y. *ACS Nano* **2007**, *1*, 258-264.

(49) Escobedo, J. O.; Rusin, O.; Lim, S.; Strongin, R. M. *Curr. Opin. Chem. Biol.* **2010**, *14*, 64-70.

(50) Luo, S. L.; Zhang, E. L.; Su, Y. P.; Cheng, T. M.; Shi, C. M. *Biomaterials* **2011**, *32*, 7127-7138.

(51) Yuan, L.; Lin, W. Y.; Zheng, K. B.; He, L. W.; Huang, W. M. *Chem. Soc. Rev.* **2013**, *42*, 622-661.

(52) Kim, E. Y., K.; Giedt, R.; Weissleder, R. *Chem. Commun.* **2014**, *50*, 4504.

(53) Egawa, T.; Hanaoka, K.; Koide, Y.; Ujita, S.; Takahashi, N.; Ikegaya, Y.; Matsuki, N.; Terai, T.; Ueno, T.; Komatsu, T.; Nagano, T. *J. Am. Chem. Soc.* **2011**, *133*, 14157-14159.

(54) Chang, C. J.; Jaworski, J.; Nolan, E. M.; Sheng, M.; Lippard, S. J. *Proc. Natl. Acad. Sci. U.S.A.* **2004**, *101*, 1129-1134.

(55) Stamler, J. S.; Simon, D. I.; Osborne, J. A.; Mullins, M. E.; Jaraki, O.; Michel, T.; Singel, D. J.; Loscalzo, J. *Proc. Natl. Acad. Sci. U.S.A.* **1992**, *89*, 444-448.

(56) Spahl, D. U.; Berendji-Grun, D.; Suschek, C. V.; Kolb-Bachofen, V.; Kroncke, K. D. *Proc. Natl. Acad. Sci. U.S.A.* **2003**, *100*, 13952-13957.

(57) Kozhukh, J.; Lippard, S. J. *Inorg. Chem.* **2012**, *51*, 7346-7353.

(58) Wrobel, A. T.; Johnstone, T. C.; Liang, A. D.; Lippard, S. J.; Rivera-Fuentes, P. *J. Am. Chem. Soc.* **2014**, *136*, 4697-4705.

(59) Lim, M. H.; Lippard, S. J. *Inorg. Chem.* **2006**, *45*, 8980-8989.

(60) Khin, C.; Lim, M. D.; Tsuge, K.; Iretskii, A.; Wu, G.; Ford, P. C. *Inorg. Chem.* **2007**, *46*, 9323-9331.

(61) Tsuge, K.; DeRosa, F.; Lim, M. D.; Ford, P. C. *J. Am. Chem. Soc.* **2004**, *126*, 6564-6565.

(62) Ouyang, J.; Hong, H.; Shen, C.; Zhao, Y.; Ouyang, C. G.; Dong, L.; Zhu, J. H.; Guo, Z. J.; Zeng, K.; Chen, J. N.; Zhang, C. Y.; Zhang, J. F. *Free Radic. Biol. Med.* **2008**, *45*, 1426-1436.

(63) Pluth, M. D.; Chan, M. R.; McQuade, L. E.; Lippard, S. J. *Inorg. Chem.* **2011**, *50*, 9385-9392.

(64) Yuan, L.; Lin, W. Y.; Zhao, S.; Gao, W. S.; Chen, B.; He, L. W.; Zhu, S. S. *J. Am. Chem. Soc.* **2012**, *134*, 13510-13523.

(65) Reddie, K. G.; Humphries, W. H.; Bain, C. P.; Payne, C. K.; Kemp, M. L.; Murthy, N. *Org. Lett.* **2012**, *14*, 680-683.

(66) Murphy, S.; Yang, X. Q.; Schuster, G. B. *J. Org. Chem.* **1995**, *60*, 2411-2422.

(67) Achilefu, S. R., R.; Dorshow, R.; Bugaj, J. U.S. Patent 6180087B1, 2001.

(68) Mayerhoffer, U.; Deing, K.; Gruss, K.; Braunschweig, H.; Meerholz, K.; Wurthner, F. *Angew. Chem. Int. Ed.* **2009**, *48*, 8776-8779.

(69) Phili, R. P., A.; Baumler, W.; Szeimes, R.M.; Abels, C. *J. Photochem. Photobiol. A.* **1995**, *96*, 137-148.

(70) Sasakura, K.; Hanaoka, K.; Shibuya, N.; Mikami, Y.; Kimura, Y.; Komatsu, T.; Ueno, T.; Terai, T.; Kimura, H.; Naganot, T. *J. Am. Chem. Soc.* **2011**, *133*, 18003-18005.

(71) Burdette, S. C.; Walkup, G. K.; Spingler, B.; Tsien, R. Y.; Lippard, S. J. *J. Am. Chem. Soc.* **2001**, *123*, 7831-7841.

(72) Chapman, G.; Henary, M.; Patonay, G. *Anal. Chem. Insights* **2011**, *6*, 29-36.

(73) Miranda, K. M.; Nagasawa, H. T.; Toscano, J. P. *Curr. Top. Medicinal Chem.* **2005**, *5*, 649-664.

(74) Philip, R.; Penzkofer, A.; Baumler, W.; Szeimies, R. M.; Abels, C. *J. Photochem. Photobiol. A.* **1996**, *96*, 137-148.

(75) Harding, J. L.; Reynods, M. M. *Anal. Chem.* **2014**, *86*, 2025-2032.

(76) Rivera-Fuentes, P., Lippard, S. J. *ChemMedChem* **2014**. DOI: 10.1002/cmdc.201400014

(77) Bullok, K. E.; Gammon, S. T.; Violini, S.; Prantner, A. M.; Villalobos, V. M.; Sharma, V.; Piwnica-Worms, D. *Mol. Imaging* **2006**, *5*, 1-15.

(78) Fonseca, S. B.; Pereira, M. P.; Kelley, S. O. *Adv. Drug Deliv. Rev.* **2009**, *61*, 953-964.

(79) Vives, E.; Brodin, P.; Lebleu, B. *J. Biol. Chem.* **1997**, *272*, 16010-16017.

(80) Chyan, W.; Zhang, D. Y.; Lippard, S. J.; Radford, R. J. *Proc. Natl. Acad. Sci. U.S.A.* **2014**, *111*, 143-148.

(81) Murphy, M. P. *Biochim. Biophys. Acta-Bioenerg.* **2008**, *1777*, 1028-1031.

(82) Smith, R. A. J.; Hartley, R. C.; Murphy, M. P. *Antioxid. Redox Signal.* **2011**, *15*, 3021-3038.

(83) Dickinson, B. C.; Chang, C. J. *J. Am. Chem. Soc.* **2008**, *130*, 9638-9639.

(84) Tomat, E.; Nolan, E. M.; Jaworski, J.; Lippard, S. J. *J. Am. Chem. Soc.* **2008**, *130*, 15776-15777.

(85) Doerr, A. *Nat. Methods* **2013**, *10*, 196-196.

(86) Srikun, D.; Albers, A. E.; Nam, C. I.; Iavaron, A. T.; Chang, C. J. *J. Am. Chem. Soc.* **2010**, *132*, 4455-4465.

(87) Wender, P. A.; Mitchell, D. J.; Pattabiraman, K.; Pelkey, E. T.; Steinman, L.; Rothbard, J. B. *Proc. Natl. Acad. Sci. U.S.A.* **2000**, *97*, 13003-13008.

(88) Duchardt, F.; Fotin-Mleczek, M.; Schwarz, H.; Fischer, R.; Brock, R. *Traffic* **2007**, *8*, 848-866.

(89) Reddy, P. M.; Bruice, T. C. *J. Am. Chem. Soc.* **2004**, *126*, 3736-3747.

(90) Dasari, M.; Lee, S.; Sy, J.; Kim, D.; Lee, S.; Brown, M.; Davis, M.; Murthy, N. *Org. Lett.* **2010**, *12*, 3300-3303.

(91) Neidle, S. *Nat. Prod. Rep.* **2001**, *18*, 291-309.

(92) Chirakul, P.; Hampton, P. D.; Bencze, Z. *J. Org. Chem.* **2000**, *65*, 8297-8300.

(93) Tomasulo, M.; Kaanumal, S. L.; Sortino, S.; Raymo, F. M. *J. Org. Chem.* **2007**, *72*, 595-605.

(94) Kirin, S. I.; Noor, F.; Metzler-Nolte, N.; Mier, W. *J. Chem. Educ.* **2007**, *84*, 108-111.

(95) Maryanoff, B. E.; Reitz, A. B.; Duhlemswiler, B. A. *J. Am. Chem. Soc.* **1985**, *107*, 217-226.

(96) Behrens, C.; Harrit, N.; Nielsen, P. E. *Bioconjugate Chem.* **2001**, *12*, 1021-1027.

(97) Zhu, S. G.; Harwood, E.; Cai, S. P.; Shang, X.; Galvin, G.; Jin, L.; Yeung, A.; Diaz, B.; Zheng, M. N.; Ryckman, D. *Chimia* **2006**, *60*, 584-592.

Curriculum Vitae

Education **Massachusetts Institute of Technology,** Cambridge, MA
Candidate for Bachelor of Science in Chemistry (2010-2014)

Research **Massachusetts Institute of Technology,** Cambridge, MA
Lippard Laboratory, Undergraduate Researcher (2011-2014)

U.S. Army Center for Health Promotion and Preventive Medicine, Edgewood, MD
Directorate of Occupational and Environmental Medicine (2008-2010)

Publications **Wrobel, A. T.**; Johnstone, T. C.; Liang, A. D.; Lippard, S. J.; Rivera-Fuentes, P. A Fast and Selective Near-Infrared Fluorescent Sensor for Multicolor Imaging of Biological Nitroxyl (HNO). *J. Am. Chem. Soc.* **2014**, *136*, 4697 - 4705.

Liang, A. D.; **Wrobel, A. T.**; Lippard, S. J. A Flexible Glutamine Regulates the Catalytic Activity of Toluene *o*-xylene Monooxygenase. *Biochemistry* **2014**, accepted.

Awards MIT Department of Chemistry Service Award (2014)
MIT Department of Chemistry ACS Inorganic Chemistry Award (2014)